

POLITECNICO DI TORINO

MASTER'S THESIS

---

# Graphene integration on highly dense and multifunctional neural probes

---

*Author:*  
Elisa D'ARPA

*Supervisor:*  
Dr. Andrea LAMBERTI  
Dr. Stefano CABRINI



*A thesis submitted in fulfillment of the requirements  
for the Master of Science degree in Nanotechnologies for the ICTs*

*in the*

Molecular Foundry  
Lawrence Berkeley National Laboratory

April 2018



# *Abstract*

The work presented in this thesis is based on the development of a multifunctional neural probe, i.e. a micrometric device able to efficiently analyse the brain and in particular study the communications between neurons. The multifunctionality of the probe is achieved integrating on the tip of the same device both an electrical part, composed of Gold electrodes, to sense the neural activity, and an optical part, composed of Silicon Nitride waveguides, used to stimulate the brain through light. The project starts with the design of the probe using a CAD tool, then the device is fabricated exploiting micro and nano machining technologies and finally both the optical and the electrical part are properly characterised.

Furthermore in the project also the integration of graphene as a surface modifier of the probe electrodes has been studied, in order to demonstrate the possible improvement in electrode impedance and biocompatibility that can be achieved thanks to this material. The growth, transfer and integration in the fabrication process of graphene have been performed, and the comparison of the results of the impedance measurements for the electrodes with and without graphene is presented, in order to demonstrate the effectiveness of the material choice.

All the work has been developed at the Nanofabrication Facility of the Molecular Foundry, the nanoscience research department of the Lawrence Berkeley National Laboratory, in Berkeley (CA).

# Contents

<b>Abstract</b>	<b>i</b>
<b>1 Introduction</b>	<b>1</b>
1.1 Nanotechnologies for neuroscience . . . . .	1
1.2 New materials for neuroscience: the role of graphene . . . . .	2
1.3 Thesis Outline . . . . .	3
<b>2 Theoretical Background</b>	<b>4</b>
2.1 Neuroscience . . . . .	4
2.1.1 Neurons: structure and working functions . . . . .	4
Action Potential . . . . .	5
Synapse . . . . .	6
Electrophysiology . . . . .	6
2.1.2 Optics and optogenetics . . . . .	7
2.2 Devices: the Neural Probes . . . . .	9
2.2.1 Metal Wire Based Neural Probes . . . . .	9
2.2.2 Silicon based neural probes . . . . .	10
Utah Si Probes . . . . .	10
Michigan Si Probes . . . . .	11
2.2.3 Polymeric Neural Probes . . . . .	11
2.2.4 Neural probes integrated with waveguides . . . . .	12
2.3 Graphene integration in neurotechnology devices . . . . .	14
2.3.1 What is graphene . . . . .	14
2.3.2 Applications of Graphene in neuroscience . . . . .	14
Graphene-based Microelectrode . . . . .	15
Graphene scaffold for neural cell cultures . . . . .	15
2.4 The structure of the probe fabricated at the Molecular Foundry . . . . .	17
2.4.1 Goals and challenges . . . . .	17
2.4.2 Detailed structure . . . . .	18
Optical system . . . . .	18
Electrical circuit . . . . .	18
Microfluidic system . . . . .	19

<b>3</b>	<b>Experimental Procedure for the Fabrication of the Probe</b>	<b>20</b>
3.1	Electrical Design . . . . .	20
3.2	Optical Design and Simulation . . . . .	21
3.2.1	Ring Resonators . . . . .	23
3.2.2	Focusing Gratings . . . . .	23
3.3	Final Design . . . . .	24
3.4	Fabrication process . . . . .	26
3.4.1	Optical probes fabrication . . . . .	26
3.4.2	Electrodes and interconnections fabrication . . . . .	27
3.4.3	Etching for shank and support . . . . .	29
	$SiO_2$ Etching Optimization . . . . .	31
<b>4</b>	<b>Graphene integration on the probes electrodes</b>	<b>34</b>
4.1	Growth of graphene . . . . .	34
4.1.1	Raman Spectroscopy of graphene . . . . .	36
4.1.2	Graphene growth optimization . . . . .	37
	Pretreatments . . . . .	37
	Change in the recipe . . . . .	37
4.2	Transfer . . . . .	40
4.2.1	Transfer of graphene on gold . . . . .	41
4.3	Integration of graphene on the pads . . . . .	42
<b>5</b>	<b>Measurements and results</b>	<b>45</b>
5.1	Optical alignment and characterization . . . . .	45
5.1.1	Optical Characterisation Results . . . . .	46
5.2	Electrical characterization of the electrodes with and without graphene . . . . .	48
5.2.1	Impedance measurements of the electrodes without graphene . . . . .	49
5.2.2	Impedance measurements of the electrodes with graphene . . . . .	51
5.2.3	In Vivo Experiments . . . . .	52
<b>6</b>	<b>Conclusions</b>	<b>54</b>
6.1	Improvement obtained . . . . .	54
6.2	Future works . . . . .	55
	<b>Appendix</b>	<b>56</b>
.1	Matlab implementation of the focusing grating . . . . .	56
	<b>Bibliography</b>	<b>58</b>
	<b>Acknowledgements</b>	<b>62</b>

# List of Figures

2.1	Structure of a neuron <i>Reprinted from [19]</i> . . . . .	4
2.2	Neuronal Action Potential. <i>Reprinted from [24]</i> . . . . .	5
2.3	Synapse structure and behaviour. <i>From <a href="http://medicalterms.info/">http://medicalterms.info/</a></i> . . . . .	6
2.4	Channelrhodopsin, a light-sensitive protein, makes possible the flow of cations inside the neuron under the excitation of a particular wavelength .	8
2.5	SEM image of the tip of a metal wire based neural probe. <i>Reprinted from [38]</i>	9
2.6	Utah-type Silicon Probes (Bhandari et al., 2010) . . . . .	10
2.7	(a) Michigan-type Silicon Neural Probe <i>Reprinted from [1]</i> . (b)Scanning electron microscopy side view of a silicon probe substrate defined using a shallow (tip) and deep (shank) boron etch-stop (above) and perspective view (below). <i>from [40]</i> . . . . .	11
2.8	(a) Structure of a totally flexible multichannel probe array. (b) 3D flexible probe array after folding. <i>From [42]</i> . . . . .	12
2.9	Multiwaguide probes for independent optical stimulation of multiple site. (a) Design of the probes, integrated with multiple channel waveguides. (b) Three input waveguides are light coupled. The three output can be distinctly identified. (c) Cross section of a single waveguide, where the core is made of <i>SiON</i> ad the cladding of <i>SiO<sub>2</sub></i> . <i>Reprinted from [2]</i> . . . . .	13
2.10	Electronic band structure of the graphene. Conduction and Valence band meet at the Dirac points. . . . .	14
2.11	Graphene-based microelectrode. <i>Reprinted from [48]</i> . . . . .	15
2.12	NSC adhesion and proliferation on graphene foam based scaffold. (a) SEM image of NSCs cultured on graphene scaffold. (b) Fluorescence image of NSCs proflikerated on graphene scaffold for 5 days. <i>Reprinted from [15]</i> . .	16
2.13	Scheme of the neural probe integrated with different layers for different functionalities. . . . .	18
3.1	Electrical circuit design on the probe . . . . .	21
3.2	Electrical circuit design - Zoom on the shank <i>Every gold electrode is connected to a gold pad on the body of the probe</i> . . . . .	21
3.3	Optical Circuit Design of the probe <i>A single mode waveguide ends into the shank with several outputs</i> . . . . .	22
3.4	Optical circuit of the probe - Zoom on the shank <i>The outputs are composed of focusing gratings, coupled to the input waveguide through ring resonators</i> . . . . .	22
3.5	Ring resonator . . . . .	23

3.6	Focusing Grating . . . . .	24
3.7	Zoom on the design of the optical part of the probe. The red areas are the one that will be exposed and after etched. . . . .	25
3.8	Design of the overlapping of the optical and electrical layers of the probe. The electrodes over the focusing gratings are moved away . . . . .	25
3.9	Starting wafer, provided by <i>Lionix</i> <sup>®</sup> . . . . .	26
3.10	Fabrication steps for the fabrication of the optical system . . . . .	27
3.11	Ring Resonator . . . . .	27
3.12	Zoom on a focusing grating . . . . .	27
3.13	Fabrication steps of the electrical system . . . . .	28
3.14	SEM images of the electrical part of the probe after lift-off . . . . .	28
3.15	SEM images of the electrical structure after the passivation. On the left it is possible to see the wire covered by the oxide, while on the right the gold electrodes have been already again exposed, removing the Oxide above them. . . . .	29
3.16	Fabrication step for the backside etching . . . . .	30
3.17	Fabrication steps for the frontside etching . . . . .	30
3.18	SEM of a released probe. <i>The body of the probe is left thicker for support and handling reasons, while the shank, which will be inserted in the brain, is much thinner</i> . . . . .	31
3.19	Formation of pillars inside the trenches which rings to the saturation of the etching . . . . .	31
3.20	XPS analysis of the materials inside the trenches after the etching with $C_4F_8$ . . . . .	32
3.21	$C_4F_8=40$ sccm, $O_2=10$ sccm <i>No formation of pillar</i> . . . . .	32
3.22	Etching with $CF_4$ results <i>The trench is completely etched and there is no formation of pillars</i> . . . . .	33
4.1	Aixtron Black Magic CVD . . . . .	35
4.2	The sample is put inside the CVD chamber . . . . .	35
4.3	Schematic of the growth kinetics of graphene on Cu <i>Reprinted from [57]</i> . . . . .	35
4.4	Graphene grown on Copper Foil, a) with 10x objective b) with 50x objective . . . . .	36
4.5	Raman spectrum of 3 points of a sample of graphene on Copper . . . . .	37
4.6	Comparison between Raman Spectrum of Graphene on Copper foil treated in acetic acid and Cooper foil trated in nitric acid . . . . .	38
4.7	Graphene growth process <i>Amorphous Cu with a native oxide layer is annealed in a hydrogen rich atmosphere at 1000 °C. The hydrogen gas reduces the native oxide layer. In the growth phase methane is introduced in the chamber, starting the nucleation and growth of graphene. Reprinted from [57]</i> . . . . .	38
4.8	Comparison between Raman Spectrum of Graphene on Copper foil treated with an annealing step and Copper foil without this pretreatment . . . . .	39
4.9	Raman Spectrum of Graphene on Copper Foil for different growing temperature . . . . .	39
4.10	Effect on the graphene growth for a run performed at 1060°C . . . . .	40

4.11	Transfer process of the graphene on the desired substrate . . . . .	41
4.12	Raman Spectrum of graphene transferred on a gold substrate . . . . .	41
4.13	Transfer of graphene sample on a wafer with the final probes . . . . .	42
4.14	SEM images of the shank of a probe after the transfer of graphene above it	42
4.15	Fabrication steps for the patterning of graphene . . . . .	43
4.16	Layout for the patterning of graphene . . . . .	43
4.17	SEM image of a graphene/gold pad, after the lithography of graphene. . .	44
4.18	Raman spectrum on the shank pads: the graphene has been correctly trans- ferred . . . . .	44
5.1	Optical setup scheme used to characterise the optical structure on the probe.	46
5.2	Once the alignment is reached, the fiber is glued to the input waveguide .	46
5.3	Images taken from the CCD: (a) Full structure illuminated with white light. (b) Changing the input wavelength of the laser, different rings are selected along the optical structure. . . . .	47
5.4	Pictures of the output spot of a h20 focusing grating, taken at height a) $5 \mu m$ , b) $20 \mu m$ , c) $50 \mu m$ . . . . .	48
5.5	Intensity plots of the output spot of a h20 grating, obtained from pictures taken at different heights from the feature itself . . . . .	48
5.6	(a) Wire bonded probe on a PCB. (b) Design of a PCB: zoom on the wire bonding part. Each probe pad can be connected to a single pad on the PCB.	49
5.7	Impedance spectroscopy of Chen et al. probe, with the impedance spec- trum and the phase spectrum ranging from 10 Hz to 10 kHz. The average impedance was $2.40 M\Omega \pm 0.52 M\Omega$ at 1 kHz. <i>Reprinted from [64]</i> . . . . .	50
5.8	SEM images of electroplated electrodes . . . . .	51
5.9	Comparison of the average impedance of electrodes with and without graphene @1000 Hz . . . . .	52
5.10	Comparison of the average impedance of electrodes with and without graphene @200 Hz . . . . .	52
5.11	Electrical signal collected from an electrode. The spikes correspond to the firing of an action potential <i>Provided by Shinya Ito UCSC</i> . . . . .	53

## Chapter 1

# Introduction

### 1.1 Nanotechnologies for neuroscience

The development of new neurotechnologies is nowadays a major topic of interest for many researches all over the world. Studying the complexity of the neural system can lead to understanding and then treating neurodegenerative diseases, as well as better comprehending how human mind works. Even though there are much efforts in the study of the brain, scientists have still lot of work to do to obtain real progresses. Brain is a really complex structure, composed by a huge amount of neurons, whose signals have to be detected and collected. Moreover the brain matter is extremely delicate and thus it is really hard to efficiently interconnect with the neurons without induce damages in the brain itself.

Nanotechnologies are a really promising field to face these challenges, since they can be a powerful instruments to interact with neural cells in a controlled manner <sup>[1,2]</sup>. Once the basic communication mechanisms of the neurons have been understood, now the neuroscientists are trying to reach deeper knowledge on the localisation of the different neurons inside the brain and how the sensory ability of the human beings are related to them. Thus they need tools to simultaneously interface different single neurons. Moreover for now the devices fabricated for this applications are integrated with active or passive components, depending on the necessity to interfere with the neurons or to just collect their signal. The new task relies on the ability to integrate this two functions in the same device, in order to allow real time studying of the neurons working under particular stimuli.

Neural probes are microstructures that form the connection between the biological neural tissues with physical devices and electronics<sup>[3]</sup>. The insertion of a neural probe allows to penetrate the brain tissues reaching neurons as close as possible, but at the same time minimising the footprint of the device on the tissue brain, reducing the risk for the patient and thus also his immune response. These characteristics make then possible better measurements of the neuronal signals, targeting specific regions of the brain and reducing the signal-to-noise ratio of the recorded activity<sup>[3]</sup>. As it will further described in 2.2.2, Michigan neural probes make also possible the integration of many electrodes on the probe, thus the simultaneous observations of the activity of a large number of cells,

increasing the accuracy of the measure<sup>[4, 5]</sup>. They can be combined in arrays and they are fabricated with micro and nano machining processes, working on a full wafer, simultaneously achieving a huge number of devices.

The project started at the Molecular Foundry looks to the fabrication of a Silicon based Michigan neural probe, combined with both active and passive components. The active components are composed of  $Si_3N_4$  optical waveguides able to bring a laser source into the brain and light up a certain number of different neurons. The passive one are a huge number of gold electrodes placed on the tip of the probe, able to detect the action potentials<sup>[6]</sup> released by the neurons. The project in the future will involve also the adding of a last functionality, i.e. some microfluidic channels able to perform localised drug delivery inside the brain.

## 1.2 New materials for neuroscience: the role of graphene

The development of the neurotechnologies led the researchers to find out new devices able to efficiently interact with the brain. The using of neural probes to minimise the footprint of the device on the brain allowed to make progresses in the neuroscience, but the scientist still have the necessity to build new devices able to improve their biocompatibility and stability in a living tissues, as well as their electrical and optical signal detection capability. For this reason researchers not only focused their study on new design and technological solutions but also on new materials strategies. This is why the use of coated electrodes started to be exploited. There are researches focused on the modification of the electrodes with conductive polymer, like PEDOT, or with carbon nanotube composite, able to reduce the recording sites impedance and improve the signal-to-noise ratio<sup>[7, 8]</sup>. The use of organic materials can reduce the neuro-inflammation response of the brain, as well as the application of soften materials, which can better match the mechanical properties of the neural tissue<sup>[9]</sup>.

A promising material which could satisfy these requirements is graphene, a flat monolayer of carbon atoms packed into a two-dimensional honeycomb lattice, whose peculiarity are basically an high conductance and mechanical strength but also good biocompatibility and transparency<sup>[10, 11]</sup>. Recently graphene transistors<sup>[12]</sup> and electrodes have been fabricated for efficiently detection of action potentials. Also flexible neural microelectrodes have been implanted on the brain surface, exploiting long-term biocompatibility and high-resolution neurophysiological recording<sup>[13]</sup>. The good neural cell adhesion on graphene-based substrates has been well studied<sup>[14]</sup>, also using it as biocompatible and conductive scaffold for the growth of neural cultures<sup>[15]</sup>.

According to these studies, in this thesis the integration of graphene as a coating on neural probe electrodes has been exploited. While usually graphene-based electrodes are obtained directly growing or transferring graphene on enough wide metal electrodes,

here the graphene has been efficiently integrated in the micro and nano fabrication process performed in the whole wafer used for the fabrication of the probes. This allowed also a direct comparison between electrodes with and without graphene maintaining the same dimensions of the probe, analysis which is missed for now in the literature. The graphene coated electrodes are then obtained with standard lithographic processes on the graphene layer transferred on the full wafer, in order to simultaneously obtain a large number of probes, each of them integrated with a huge number of electrodes on their shank.

### 1.3 Thesis Outline

This thesis is divided in four main parts:

The first part is devoted to the theoretical background needed to understand how the brain basically works and so which kind of devices it requires in order to be efficiently analysed and further treated. The state of the art about the Neural Probes is then presented, as well as the achievement reached in the integration of graphene in the neurotechnologies. Finally the Neural Probes thought at the Molecular Foundry is described, explaining the main reasons on which is based.

The second part concerns the design prerequisites of the probes and the fabrication steps performed on the whole wafer. All the step starting from the full substrate to the release of each single probe are described, pointing out the optimizations required during the process.

The third part of the thesis is related to the graphene integration on the probes. It starts with the study of the growth and transfer of the material, with the description of the different tests performed to obtain a better material. At the end the full transfer of graphene on the wafer already prepared with the probes is obtained and the fabrications of the electrodes through a lithographic process is shown.

Last part exposes the optical and electrical measurements performed on the probes, with and without graphene, obtaining a useful comparison between standard electrodes and surface modified one. The conclusion about the achievement obtained and the future development are finally presented.

## Chapter 2

# Theoretical Background

## 2.1 Neuroscience

Neuroscience means the study of the nervous system, from its molecular and cellular structure, to how it works in terms of communication and cognition<sup>[16]</sup>. The progress reached in the last century in the neuroscience has made possible a deeper knowledge on the interactions between neuronal cells and their reactions to specific stimuli. The basic way to perform this study is to insert small devices in the brain of living animals or grow cellular cultures which simulates the neural behaviour and then submitted them to different kind od stimuli. These stimuli induce the release of signals from the brain itself, which can be collected and elaborated in order to obtain information on the neuronal activity<sup>[17]</sup>.

### 2.1.1 Neurons: structure and working functions

The basic cell of the nervous system is the neuron. Its task is to receive and transduce information from the internal and external environment, generating a response to each stimulus<sup>[18]</sup>.

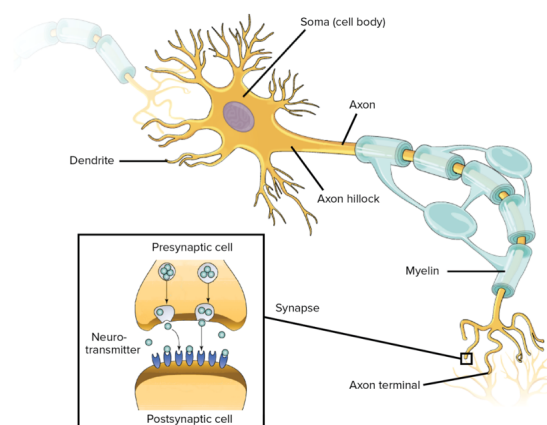


FIGURE 2.1: Structure of a neuron  
Reprinted from [19]

A neuron, depicted in figure 2.1, is basically composed of three parts:

- The body, called soma, which contains the nucleus and all the cellular organelles, able to receive the signals coming from the dendrites and transduce them in nerve pulse. It usually has dimensions between few  $\mu m$  and  $20 \mu m$ <sup>[20]</sup>.
- The dendrites, multiple short structures around the body, which get information from other neurons or receptors and send them to the soma. They usually have protrusions, in order to enlarge surface area and reach multiple neurons.
- The axon, single long structure which makes possible the travel of the nerve pulse from the body to the extremity of the neuron itself<sup>[21]</sup>.

Between the dendrites of a neuron and the axon of the another one there is a small gap, about  $200 \text{ \AA}$  wide, called synapse, where all the chemical processes happen.

The way neurons communicate through themselves is then electrochemistry.

### Action Potential

An action potential, i.e. an electrical pulse, travels through the axon and reaches its synapse<sup>[22]</sup>. Here there is a release of chemicals, which in turn reaches the dendrites of another nearby neuron. These chemicals bind then to the soma of the second neuron, inducing the opening of its membrane channels. Indeed, when a charge binds to the membrane of the soma, the voltage differences across it changes. If the voltage overcome a certain threshold, about  $15 \text{ mV}$  above the resting potentials, it makes the membrane permeable to some ions, basically sodium and potassium ions, which flow across the membrane to restore the equilibrium<sup>[23]</sup>. This lead to the sending of a peak of current out of the cell, i.e. to the raise of another action potential which again will start travel through the axon towards the synapse.

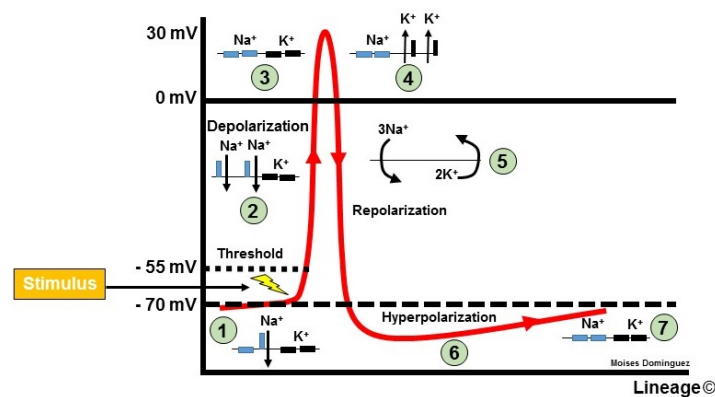


FIGURE 2.2: Neuronal Action Potential.  
Reprinted from [24]

## Synapse

The chemicals released at the synapse are called neurotransmitters: they are proteins, like adenosine, dopamine and serotonin, kept inside vesicles placed at the axon terminal<sup>[25]</sup>. At the end of an axon potassium and sodium channels are substituted by calcium channels, which are activated when there is a certain electrical activity in the pre-synaptic neuron. The opening of the channels lets the flow of  $Ca^{2+}$  ions inside the axon terminals: the ions bind the neurotransmitters vesicle, braking them and letting the release of their content. The neurotransmitters bond the post-synaptic membrane, provoking a new stimulus on the post-synaptic neuron.

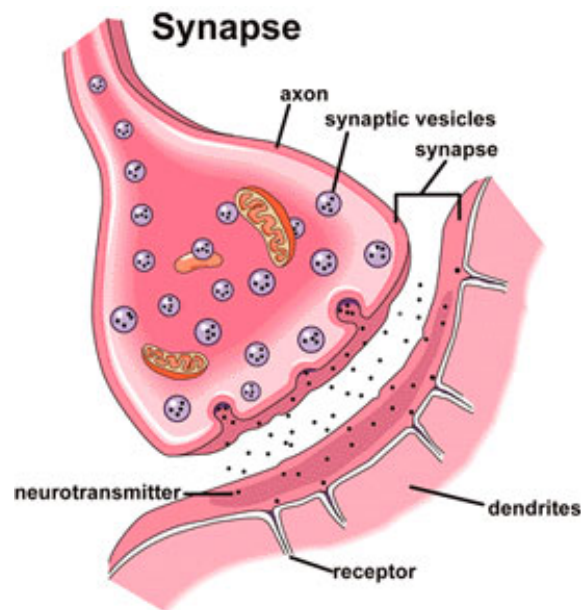


FIGURE 2.3: Synapse structure and behaviour.  
From <http://medicalterms.info/>

## Electrophysiology

The electrical signals can be recorded from the neuroscientists in two ways:

- intracellular recording: the signal is collected using a sharp tip inserted in the neuronal cell
- extracellular recording: when there is no penetration of the neuronal cell but only interface between an electrode and the tissue

The recording performed by the neural probes developed in this project is an extracellular one, which is the most suitable method to perform *in vivo* experiments, even though the signal to be measured is much lower than the intracellular one, around  $100 \mu V$ . Furthermore, while intracellular recording is usually obtained from one cell at a time and

so can give only information about the working of a single neuron<sup>[26]</sup>, extracellular one deals with the interaction of a neuron with its external environment, and so can be used to study communicational and computational capability of the neurons. Even if the extracellular spike amplitude decreases rapidly with the distance, nowadays it is possible to place electrodes really close to the neuron, with submillimeter resolution thanks to the recent microelectrode technology<sup>[27]</sup>. Moreover it is possible to fabricate arrays of microelectrodes in order to perform high density recordings of electric field of the brain, sensing a large number of neurons in parallel<sup>[28]</sup>. This also allows a triangulation of the neuron since the amplitude of the recorded spike is a function of the distance between the neuron and the electrode<sup>[29]</sup>.

Once the signal is recorded is then possible to separate different spikes, i.e. the signals coming from each neuron, and correlate it to different neurons in time and space, achieving knowledges on the travelling of information in the neural circuit.

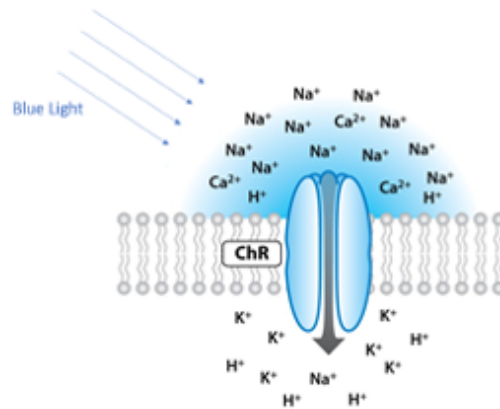
Once all the neurons are sorted, they can also be grouped depending on their functionality. Studying the different field potential shape and duration it is possible to identify the type of neurons interfaced by the probe<sup>[30]</sup> and reach deeper knowledge about the reasons brain acts in a certain way, with a particular focus on understanding how the perception of the living beings works.

### 2.1.2 Optics and optogenetics

Despite its main role on the studying of the nervous system, the analysis of the extracellular electrical signal is not enough to deeply understand the working principles of the brain. In particular it is not suitable to inhibit neurons, as well to enhance their working, unless to perform general stimulation of the brain. But also in this case the stimulation is not able to target specific type of neurons, so it lacks in selectivity. This need pushed the neuroscientists to find out new method to analyse the brain which allow time resolution and cell selectivity.

Thus the method used to manipulate specific neurons, firstly proposed by Crick<sup>[31]</sup>, is through the use of light.

The process involves the activation of specific types of photosensitive proteins that can be found on the cell membrane. The activation implicates the closing or opening of light-gated ion channels of the soma membrane of a neuron: specific atoms or molecules can then flow from one side to the other of the membrane, establishing a difference of potentials across it which can enhance or inhibit the firing of new action potentials. An example of photosensitive protein is channelrhodopsin, reported in figure 2.4, an opsin which can be excited by blue light (wavelength around 480 nm). This kind of proteins can be linked to the ion channels, for example they can be carried by viral vectors<sup>[32]</sup>, and once lighten up with the correct wavelength, they can open the ion channels<sup>[33]</sup> allowing the conduction of cations inside the neurons, which in turn enhance the release of action potentials.



 Fenno L, et al. 2011.  
Annu. Rev. Neurosci. 34:389–412

FIGURE 2.4: Channelrhodopsin, a light-sensitive protein, makes possible the flow of cations inside the neuron under the excitation of a particular wavelength

Thanks to optogenetics it is then possible to rapidly manipulate the neuronal circuit. Different type of photosensitive proteins can be linked to different kind of neurons. Therefore defined neuronal populations can be controlled with high temporal and spatial resolution, targeting specific areas of the brain just activated or inactivated one type of neurons at a particular wavelength, leaving the others unaltered<sup>[31, 34]</sup>.

To efficiently stimulate neurons through light, it is necessary to locally deliver it in the brain areas of interest. Typical methods are the use of fibers coupled to a laser source and inserted in the brain through chronically implanted cannulas<sup>[35]</sup> or fiber-coupled high-power LEDs<sup>[36]</sup>. While these methods are able just to activate or deactivate specific area of the brains, it would be more effective to build up tools able to both deliver light to the neurons and at the same time collect their electrical response to the stimulus or enlightening the electrical work of particular type of neurons deactivated the other one. This can allow the researchers to a better comprehension of the cause-effect relation on which the neural signal is based. This is what the Neural Probe fabricated at the Molecular Foundry is proposing to do.

## 2.2 Devices: the Neural Probes

According to the needs of the neuroscientists presented in 2.1, a device able to efficiently interact in vivo the brain must satisfy some basic requirements:

- *Stiffness*: it has to be hard enough to penetrate the brain tissue reaching neurons as close as possible
- *Dimensions*: it has to minimize its footprint and so the tissue damages
- *Resolution*: it has to be able to observe simultaneously a large number of cells, but maintaining a single cell resolution
- *Stability*: the mechanical properties mismatch between the device and the brain has to be minimize
- *Impedance*: the electrode impedance must allow the reading of low signals
- *Biocompatibility*: the immunologic response against the device has to be minimised
- *Multifunctionality*: different functionalities has to be implemented on the same device
- *Reproducibility*: the device has to be reproduced for mass production

The most efficient device able to satisfy these requirements is the neural probe. Depending on the material used for their fabrication, neural probes can be classified in metal wire based neural probes, Silicon based neural probes or polymeric neural probes. They can be integrated with a set of electrodes for the recording of the neural signal or can also host optical features for the stimulation of the brain.

### 2.2.1 Metal Wire Based Neural Probes

The first implemented neural probes were simply composed of metal microelectrodes (fig 2.5). They consists of a wire sharpened through wet etching in order to have a tip small enough for the cellular study<sup>[37]</sup>. The diameter of the electrode is usually around

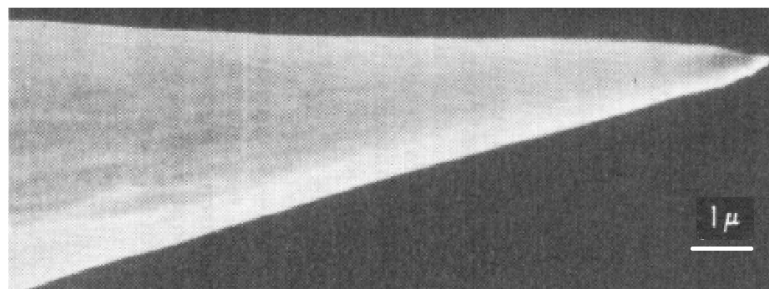


FIGURE 2.5: SEM image of the tip of a metal wire based neural probe.  
*Reprinted from [38]*

100  $\mu\text{m}$  and the wire is completely insulated except for the upper part of the tip, which will be the recording site. Even their really simple fabrication process, the dimensions of this device represent a big disadvantage: indeed the detection of a single neuron signal is not possible and the tissue damages are not negligible.

## 2.2.2 Silicon based neural probes

Silicon probes are currently the most exploited types of probes. They have millimetric dimension and are integrated with micrometric structures, obtained with standard fabrication processes. They are relatively low cost and can be produced for the large-scale. Different functionalities can be integrated on them, from electronic and optical to chemical one, thanks to the use of Silicon lithographic process, able to defined nano and micrometric structures with high precision. The standard fabrication of Si based probes exploits the deposition of a metal layer on an insulated substrate. The metal is then patterning in order to obtain the shape of the recording sites, of the pads used to connect to the external macro world and of the connection between these two features. Another insulating layer is then deposited on the probes, to passivated all the connections while leaving exposed the recording sites.

The main two types of Silicon neural probes are Utah-type Si probes and Michigan-type Si probes.

### Utah Si Probes

The Utah-type probes, depicted in figure 2.6 are arrays of vertical sharp tips directly obtained from bulk micromachining techniques, i.e. etching the Silicon wafer along its depth<sup>[39]</sup>. They can host a large number of recording sites, one per tip of the vertical pillars, but the integration of other functionalities is difficult. Moreover they have short tip length, limited by the bulk substrate thickness, so can only be used used for cortical studies, where a deep penetration is not required. Typically Utah probes array are made from

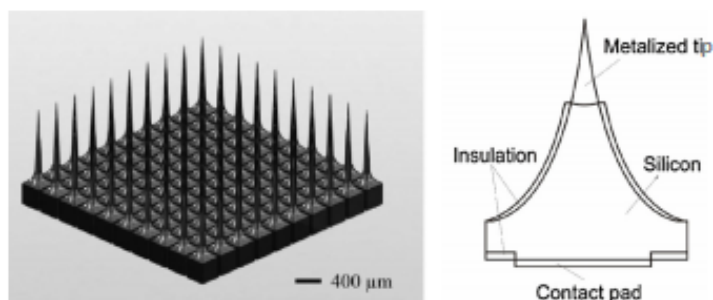


FIGURE 2.6: Utah-type Silicon Probes (Bhandari et al., 2010)

1.83 mm thick boron doped Silicon wafers. The structures are obtained using a diamond dicing saw, which firstly patterns the substrate with a grid of 300  $\mu\text{m}$  deep grooves. The

electrodes bases are insulated one from the others with the deposition of a sealing glass on the grid. Then the vertical pillars are created by sawing the grid on the other side of the Silicon wafer. The probes are sharpened with acid etching and then are coated with metals suitable for recording and stimulation of neurons (e.g. Gold and Platinum). The probes surface, except for the recording sites, is then covered with polyimide, to ensure a good insulation.

### Michigan Si Probes

The Michigan-type probes, shown in figure 2.7, are obtained lying down on the substrate, horizontally oriented. The recording sites are obtained with deposition and patterning of metal layers on the wafer. The shape of the probes is fabricated exploiting anisotropic etching, usually ethylene diamine pyrocatechol (EDP) one: the etching rate is different in case of undoped Silicon or p-type Silicon, where it is much slower, thus first Boron diffusion is performed on the wafer to define the probes shaft area, i.e. the area where the recording sites will be placed, and then EDP wet etching is used to release the probes. The thickness of the device can be further reduced using deep reactive ion etching. The insulation layers on top of the Silicon substrate is obtained with a triple layer of  $SiO_2 - Si_3N_4 - SiO_2$ . Further electronics can be added on the upper part of the probes, thicker, in order to obtain an active device, able to amplify and demultiplex the signals.

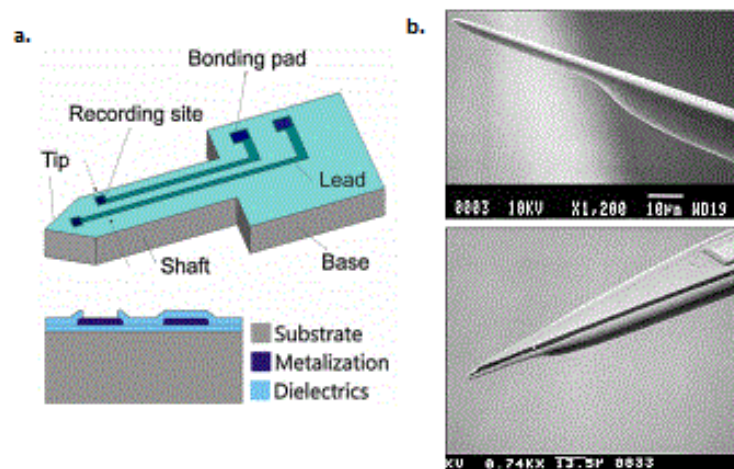


FIGURE 2.7: (a) Michigan-type Silicon Neural Probe *Reprinted from [1]*. (b) Scanning electron microscopy side view of a silicon probe substrate defined using a shallow (tip) and deep (shank) boron etch-stop (above) and perspective view (below). *from [40]*.

### 2.2.3 Polymeric Neural Probes

The main issue regarding Silicon implanted neural probes is the stability and the biocompatibility of the device: Silicon is much stiffer than the brain tissue and the immune

response against the device limits a good reading of the signals. In order to mitigate this problem, neural probes coated with softer polymers, as Polyimide<sup>[41]</sup> and Parylene-C<sup>[1]</sup>, have been fabricated. Also totally flexible probes arrays have been developed employing flexible materials such as SU-8, polyimide or PDMS<sup>[42]</sup>, exploiting lithography, micro-molding or dry etching techniques. Depicted in figure 2.8, they are obtained starting from a plain polymeric substrate which is patterned to obtain the 2D probes shape. At this stage multiple electrodes and interconnections are created on each probe. Placing a magnetic thin plate on the backside of the devices, it is then possible to stand up the probes using an external magnetic field, so that the final result is an array of vertical flexible probes, with recording pads at different heights along the shank. Since they can deform their shape without the creation of fractures, they can be efficiently implanted in the brain limiting its damages.

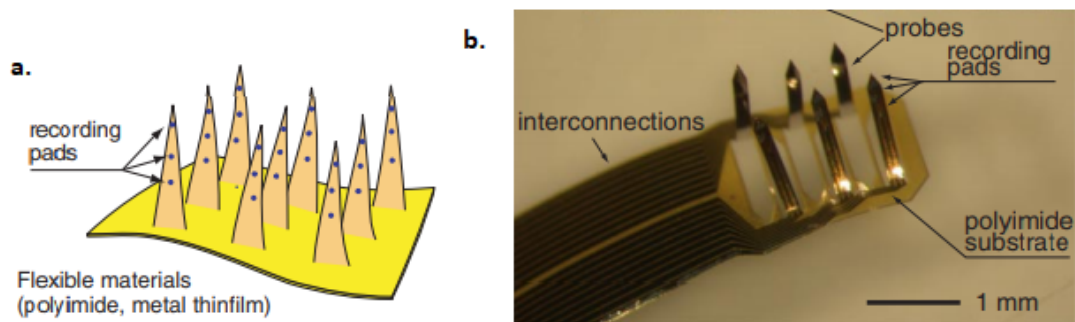


FIGURE 2.8: (a) Structure of a totally flexible multichannel probe array. (b) 3D flexible probe array after folding.  
From [42]

The flexibility of these probes reduce the footprint of the device in the neural tissue, but at the same time the lack of rigidity can causes buckling during the implantation. Thus long length polyimide probes can not be used and this is why even their drawbacks, Silicon based neural probes remains the most useful tool for an efficiently study of the brain.

#### 2.2.4 Neural probes integrated with waveguides

Neural probes for in vivo optogenetic experiments have been already developed with the integration of photonic waveguides on the devices. The probes are Silicon based one and involve the adding of a layer, properly patterned, where the optical features are fabricated. The materials used are typically SiN<sup>[43]</sup> or SiON<sup>[44]</sup>, and the fabrication techniques used are common micromachining processes as PECVD, lithography and dry etching. Different structures can be exploited on the optical probes in order to reach different areas of the brain with single cell resolution, using more than one input waveguides which can be independently lighted up<sup>[45]</sup>, or alternatively a single input waveguide which can ends with multiple stimulation sites thanks to the use of demultiplexer<sup>[46]</sup>, in order to minimise the dimensions of the shank to be inserted in the brain. The structure of a

neural probe integrated with multichannel waveguides for the independent optical stimulation of multiple sites is reported in figure 2.9.

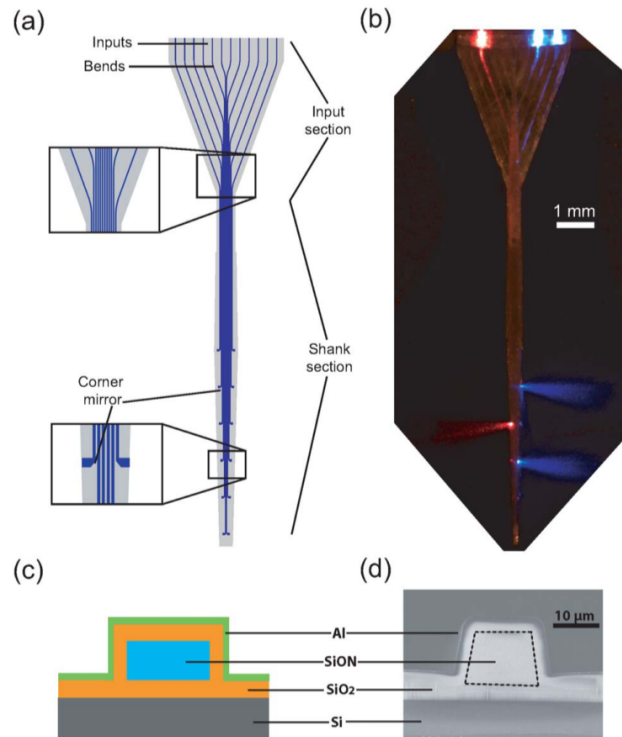


FIGURE 2.9: Multiwaveguide probes for independent optical stimulation of multiple sites.

(a) Design of the probes, integrated with multiple channel waveguides. (b) Three input waveguides are light coupled. The three output can be distinctly identified. (c) Cross section of a single waveguide, where the core is made of  $SiON$  and the cladding of  $SiO_2$ .

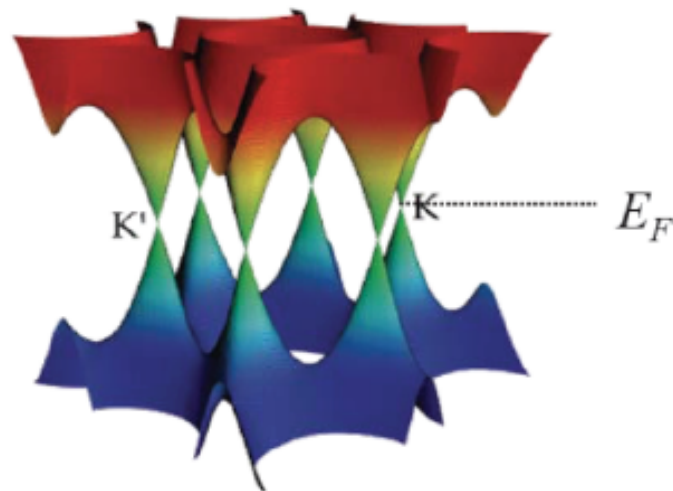
*Reprinted from [2]*

## 2.3 Graphene integration in neurotechnology devices

### 2.3.1 What is graphene

Graphene is an allotropic form of carbon made up of a flat monolayer of carbon atoms packed into a two-dimensional honeycomb lattice<sup>[47]</sup>.

Currently graphene is one of the most studied material, because of its powerful potential in many applications, from electronics, to bio-sensing, membrane technology and battery technology. The electronic structure of graphene shows that the material has a linear dispersion relation near the Fermi energy, so that the conduction and valence band meet at some point, called Dirac points, at the edge of the Brillouin zone (fig. 2.10). This makes graphene a so called zero-gap semiconductor, with obvious implications in the electron mobility, even at room temperature, and conductivity of the material.



P.R. Wallace, *Phys. Rev.* **71**, 622 (1947)

FIGURE 2.10: Electronic band structure of the graphene. Conduction and Valence band meet at the Dirac points.

The interesting properties of graphene are not only limited to the electrical one. Indeed, it has great characteristics in terms of transparency, heat conduction and mechanical properties, which make it a hard but flexible material. It is chemically inert, making it suitable for application which requires high stability.

### 2.3.2 Applications of Graphene in neuroscience

The employment of graphene in neuroscience is due not only to its good conductivity, mechanical strength and transparency, but also and in particular because its proven biocompatibility and low toxicity.

### Graphene-based Microelectrode

Recently graphene has been used to fabricate transistors and electrodes exploited to detect action potentials. Graphene, grown on Copper foil, is transferred to a Silicon Dioxide substrate using a sacrificial polymer layer and then the sharp-edged probe is obtained using manual dicing. The wiring between the graphene pad and the PCB is performed thanks to a gold line of diameter of 0.1 mm<sup>[48]</sup>. The insulating layer is then obtained with a coating of PDMS on the probe. Even if with this technique the dimensions of the

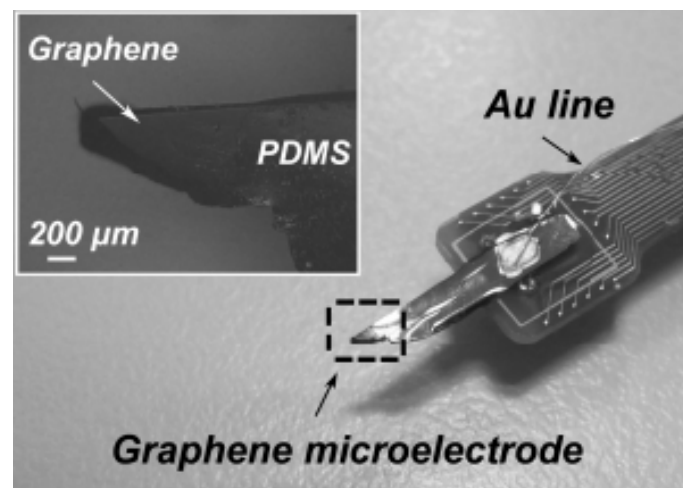


FIGURE 2.11: Graphene-based microelectrode.  
*Reprinted from [48]*

electrode are not as small as the one integrated on the common neural probes and it is difficult to have several graphene electrodes on the same device, the results of the neural recording demonstrate that the microelectrode is able to efficiently detect action potentials, with a high SNRs. The work thus allows to further transfer of graphene on other arbitrary substrates, developing also microelectrode arrays for neural recording.

Other studies have demonstrated that graphene can be also transferred on transparent substrates such as parylene C, polyethylene and polyimide, in order to obtain transparent electrodes achieving a better imaging of the area under the electrodes<sup>[11]</sup>.

### Graphene scaffold for neural cell cultures

In addition to the results in the detection of action potentials, graphene has been exploited also in the fabrication of scaffold for neural tissue cultures, showing an improvement in terms of cells adhesion and 3D growth of neural networks on it<sup>[15]</sup>. A 3D porous structure composed of graphene foam has been developed as a scaffold for Neural stem cell (NSC) in vitro. It has been demonstrated that the scaffold is able not only to support the growth of the NSC, but also to keep the cells in an active proliferation state. In this way 3D graphene scaffold can be a powerful platform for neural regeneration therapy.

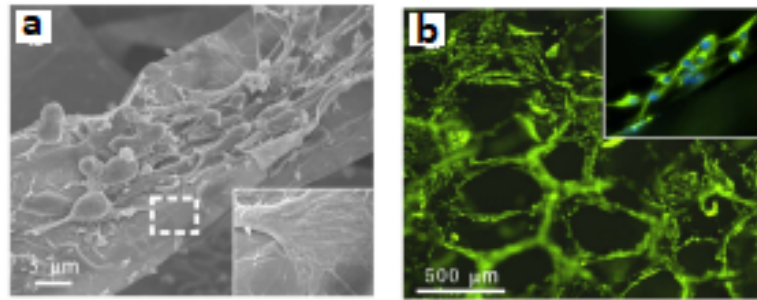


FIGURE 2.12: NSC adhesion and proliferation on graphene foam based scaffold. (a) SEM image of NSCs cultured on graphene scaffold. (b) Fluorescence image of NSCs proliferated on graphene scaffold for 5 days.

*Reprinted from [15]*

Finally other group have used graphene also in the developing of FETs setup for recording of action potentials from cultured cardiomyocytes: the cells have been directly grown on graphene-FETs arrays demonstrating a high SNR during the recording, but also a strong electrochemical stability at the cell-graphene interface<sup>[49]</sup>.

## 2.4 The structure of the probe fabricated at the Molecular Foundry

The Neural Probe fabricated at the Molecular Foundry is a Michigan-type Silicon probe, so it is composed of a long but thin shank for the insertion in the brain, hosting a high number of recording and stimulating sites, and an upper part for PCB connection and handling.

The project started in 2016, with the study of the design of the probe and of the material suitable for its fabrication. The original team was composed of three people of the Nanofabrication facilities of the laboratory, but after involved also other users, especially master students, for shorter or longer periods. Moreover collaborations with other research groups have been established, as for example with the University of Berkeley and the University of Santa Cruz, especially for the *in vivo* experiments, all performed by neuroscientists working outside the Molecular Foundry.

### 2.4.1 Goals and challenges

The main goal of the project at the Foundry is to build up a device able to simultaneously provide as much information as possible from the brain. For this reason, the probe is a multifunctional one, so it exploits both an electrical part for the detecting of the neural signals and an optical one to actively interfere the neurons. The two systems are exploited in two layers integrated in the some device, so that it is possible to interact with the neurons and collecting in real time their response toward the stimulus. Such device can then overcome the limits of the standard neural probes, which are usually devoted to only a particular function, detection or stimulus.

The choice of a Michigan-type probe is because it is possible to reduce the damages of the brain tissue during the insertion and so the immune response against the device. Moreover they are fabricated with standard micro and nanofabrication processes, so that it is possible to work in parallel on a large number of probes placed on a full wafer, allowing a large-scale production of the device.

Finally, to enhance the biocompatibility of the probe, which turns in a better adhesion between the device and the neurons and a reduction of the immune response, and to improve the electrodes impedance, which has to be minimised to efficiently read the neural signals, the integration of a graphene layer on the electrodes of the probe has been studied. Graphene has been widely used for the fabrication of electrodes devoted to action potentials detection, but they are usually wide and not simultaneously fabricated in a large number. The idea used in this project is instead to integrate graphene in the full fabrication process, so to use a wafer-sized graphene layer transferred on the wafer prepared with the probes and then to perform standard lithographic and etching processes for its patterning. In this way it is possible to obtain a wide number of smaller graphene electrodes, integrated in the same device, working simultaneously on a large number of devices on the wafer, leading thus to a large-scale production of graphene based micro-electrodes too.

### 2.4.2 Detailed structure

The probe is composed of a  $45\ \mu\text{m}$  wide and 1 mm long shank and a wider and thicker body used as support. The shank hosts a large number of recording sites able to interfere neurons at different positions in the mice's cortex.

Each functionality exploited is integrated in the probe in different layers stacked one over the other and separated by insulating layers. The actual probe is composed of a first layer for the optical features, and a second one for the electrical circuit. In the future another layer will be added to the probe for the integration of microfluidic channels able to provide local drug delivery inside the brain<sup>[50]</sup>.

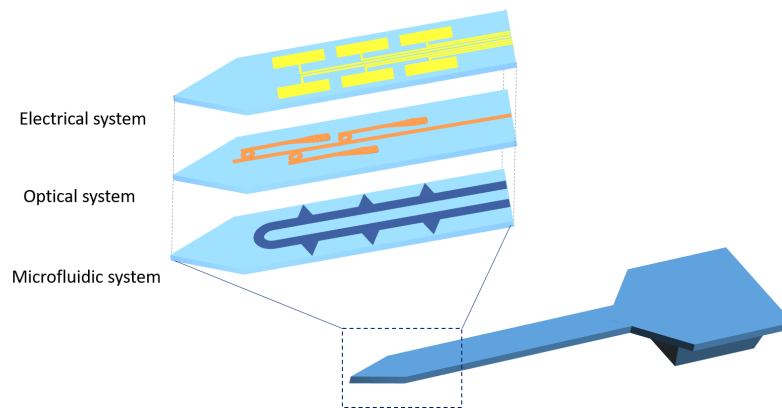


FIGURE 2.13: Scheme of the neural probe integrated with different layers for different functionalities.

#### Optical system

The optical system is exploited in the lower layer of the probe. It is composed of a single input  $\text{Si}_3\text{N}_4$  waveguide which ends in the shank with several outputs, consisting in focusing gratings able to focus light at a certain height. The gratings are coupled to the waveguide with different ring resonators, which allow the passing only of a specific wavelength, so that the grating can be selectively activated just changing the input wavelength.

#### Electrical circuit

The electrical circuit is composed of 64 gold electrodes placed on the shank and connected to the pads on the body through 100 nm thick wires. The body is then wire-bonded to a printed circuit board (PCB). The electrodes are vertically aligned in two lines along the edge of the shank, in order to maximize the number of recording sites, and so the neuronal area interfered, while maintaining small width of the device. The electrodes are then coated with graphene layer or alternatively electroplated with a Gold electroplating solution.

**Microfluidic system**

The microfluidic system thought for the project will be made of a u-shaped microchannel which will travel along the shank. The drugs pumped inside the channel will be released through several outputs placed along the channel, which will be selectively opened thanks to an electrosmotic pumping system.

## Chapter 3

# Experimental Procedure for the Fabrication of the Probe

The project developed at the Molecular Foundry consisted in the design and fabrication of high density and multifunctional neural probes, fabricated on 4 inches wafers, in order to obtain simultaneously a large number of devices (more than 150 probes per wafer).

Firstly the pattern of the probes is decided with the fabrication of the lithographic masks for the full wafer. Further both the electrical and optical circuit to be obtained on every probes are designed with a CAD tool.

Once the design is chosen and optimized, it is fabricated on the full wafer through several cleanroom steps, each of them has to be optimized.

Finally, when the probes are completed and released from the wafer, they have to be characterised, using a suitable optical and electrical set up.

The work carried on during my stay has been focused on the characterisation of the optical elements of the probe and the optimization of the fabrication processes, in particular the one related to the last etching of the backside and frontside of the probes, needed before their release, as it will be explained in the next sections. The current team, composed by me, another master student and a PhD student, took turns to perform all the fabrication and the characterisation at each process step of the probe.

At the same time I personally developed the process for the integration of graphene on the probe electrodes, working at the Inorganic Materials facility of the Molecular Foundry for the growth of the material and then performing the transfer and the patterning on the probe inside the cleanroom of the Nanofabrication facility.

### 3.1 Electrical Design

The electrical system of the probes is designed using *L-Edit*, a CAD editor for the fabrication of integrated circuit.

The shank of the probe, shown in figure 3.2, hosts 64 rectangular gold electrodes of dimensions

$$\text{Area} : 5 \times 25 \mu\text{m}^2$$

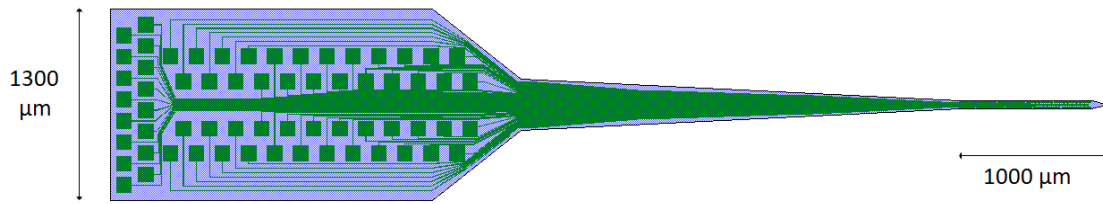


FIGURE 3.1: Electrical circuit design on the probe

with a distance of  $2.5 \mu\text{m}$  one from the next one. These dimensions allow the integration of a huge number of electrodes on the same probe and also the interaction with single neurons during in vivo experiments, since the dimensions of a neuron are comparable to the one of the electrodes.

Each electrode is connected to a squared gold pad placed in the body of the probe, of dimensions

$$\text{Area} : 100 \times 100 \mu\text{m}^2$$

The gold connection wires are  $120 \text{ nm}$  wide and connect a single electrode to a single pad. This wire width is required to allow the fabrication of a high density interconnection pattern, able to bond the large amount of pads and electrodes hosted by the probe. The

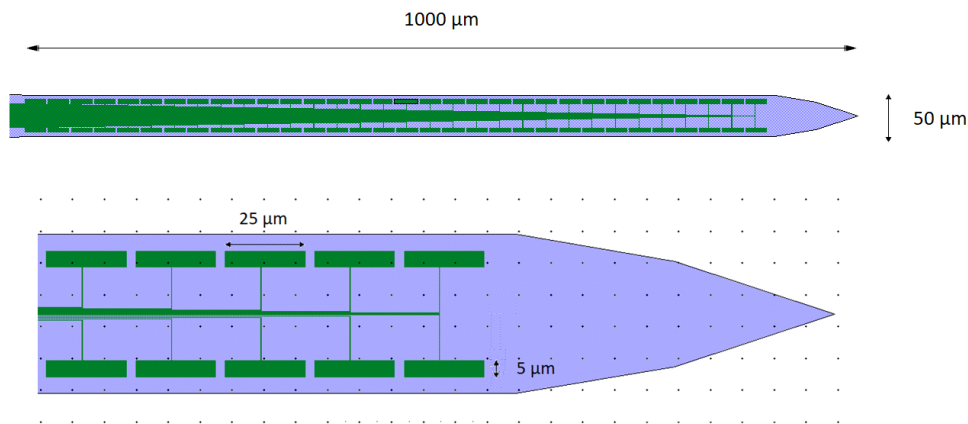


FIGURE 3.2: Electrical circuit design - Zoom on the shank  
Every gold electrode is connected to a gold pad on the body of the probe

overall dimensions of the shank are  $1 \text{ mm}$  of length, which represents the thickness of mice cortex,  $50 \mu\text{m}$  of width and  $20 \pm 50 \mu\text{m}$  of depth, to minimise the brain damage.

### 3.2 Optical Design and Simulation

The optical part is composed of  $\text{Si}_3\text{N}_4$  waveguides, claded by a  $\text{SiO}_2$  layer. They start from the body of the probe with a single input waveguide and end into the shank with

several outputs.

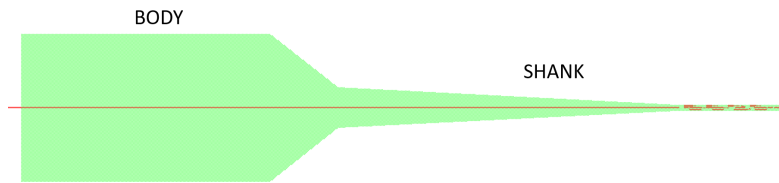


FIGURE 3.3: Optical Circuit Design of the probe  
A single mode waveguide ends into the shank with several outputs

$Si_3N_4$  and  $SiO_2$  are optimal materials for optogenetics since they have a low absorption and low losses in the range of wavelengths required, from visible to near infrared, a range which includes the wavelength able to excite channelrhodopsin<sup>[27]</sup>.

To correctly choose the correct geometrical dimensions of the optical design, every structure is simulated using *Lumerical FDTD*<sup>®</sup>, a software able to solve Maxwell's equations for each point of the simulation grid, performing a Finite-difference time-domain calculation.

The first constrain to be satisfied is that the waveguide has to be single mode, in order to be correctly coupled to the ring resonators, one of the main feature of the optical structure. Knowing the refractive indices at  $\lambda = 450 \text{ nm}$  for  $Si_3N_4$  ( $n_{core} = 2.0786$ ) and  $SiO_2$  ( $n_{clad} = 1.4656$ )<sup>[51]</sup> and fixing the thickness at 160 nm, which is the thickness of the Nitride layer of the wafer used in the fabrication process, from the simulation the width of the waveguides results to be in the range  $[280 \div 340] \text{ nm}$ . The overall refractive index of the structure is then  $n_{eff} = 1.75$ .

The outputs of the optical design are obtained using two main elements: ring resonators and focusing gratings.

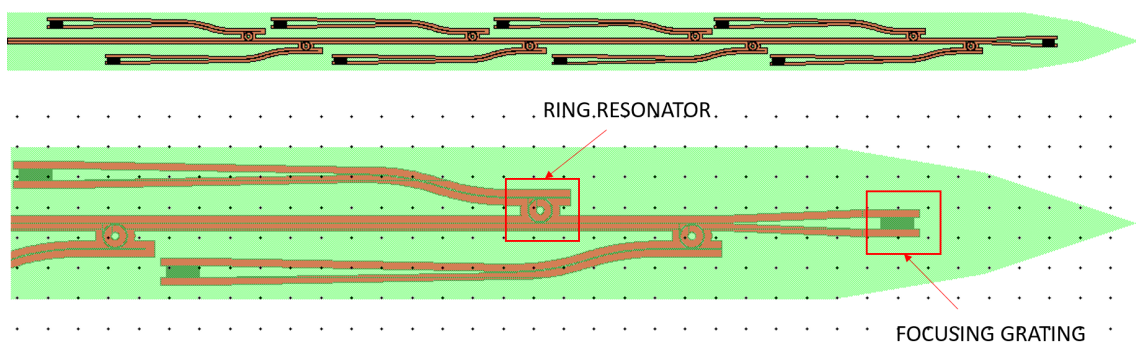


FIGURE 3.4: Optical circuit of the probe - Zoom on the shank  
The outputs are composed of focusing gratings, coupled to the input waveguide through ring resonators

### 3.2.1 Ring Resonators

Ring resonators are optical elements able to filter a specific wavelength and propagate it to the next waveguide. The selected wavelength depends on the radius of the ring itself, since a stationary wave can arise in the resonator only if its wavelength is a submultiple of the circumference of the ring itself. Then just tuning the dimensions of the element it is possible to select different wavelengths.

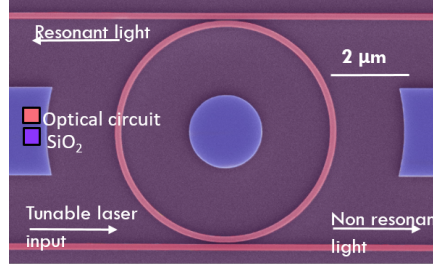


FIGURE 3.5: Ring resonator

The dimensions of the ring are chosen using the equation 3.1, imposing a FSR greater than 4 nm.

$$R \leq \frac{\lambda^2}{n_{eff} 2\pi FSR} \simeq 4.6 \mu m \quad (3.1)$$

Using these geometrical parameters, a 3D model of the ring resonator is created and simulated with *Lumerical*, to test the correct behaviour of the element in the wavelengths range of interest. Placing rings with different radius along the shank of the probe it is then possible to illuminate different brain area. The light at a particular wavelength travels along the input waveguide and reaches the ring resonators, entering only the ones designed for that particular wavelength, while passing over the other ones. Thus the light switches from the input waveguide to the other optical branches, reaching different gratings in different areas of the shank. When the input wavelength changes, these gratings switches off since the light will not be coupled to the respectively ring resonator, but instead will enter other optical branches passing through other ring resonators. In this way the light will interferes different neurons near the probe.

### 3.2.2 Focusing Gratings

Focusing gratings are gratings able to output light and focus it at a certain distance. They are then used to extract light from the probes and deliver it to the neurons. The power of these elements is that, since the insertion of the probe induces cellular damage in the brain tissue just around the device, having light focused at a certain distance may ensures the interaction only with neurons not killed by the probe itself.

The grating is composed of a series of bent grooves of thickness  $\frac{\lambda}{2 \cdot n_{eff}}$ . The geometrical parameters of the grating are chosen so that all the light interferes constructively in

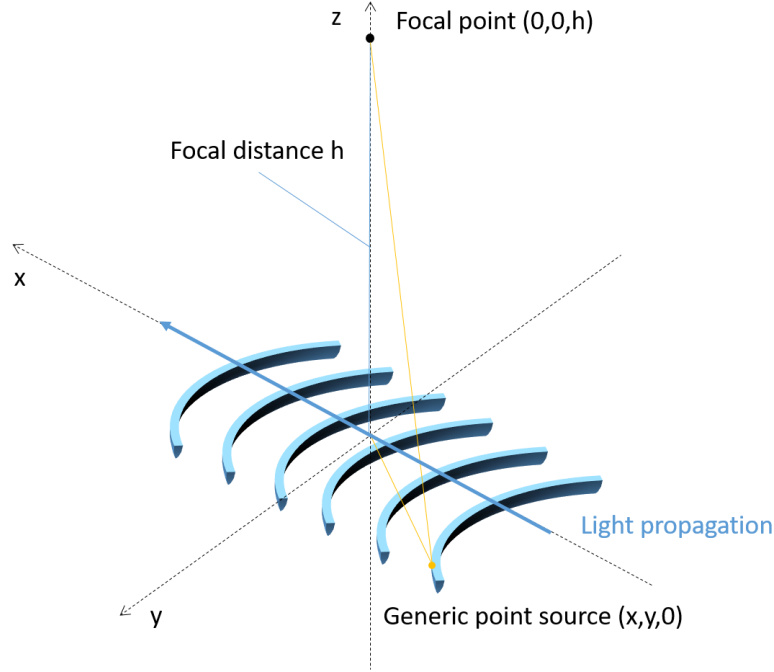


FIGURE 3.6: Focusing Grating

the desired focal point. Each point of the groove edge is like a point source of light, then in order to have constructive interference all the light emitted must have the same phase. For a generic point  $(x, y, 0)$ , this constrain is ensured if equation 3.2 is satisfied

$$\sqrt{x^2 + y^2 + h^2} + x \frac{n_{eff}}{n_m} = m \frac{\lambda}{n_m} \quad (3.2)$$

where  $h$  is the focal distance,  $n_{eff}$  is the effective refractive index of the grating,  $n_m$  is the refractive index of the medium around the grating and  $m$  is a natural number. Selecting all the point  $(x, y)$  that satisfies the equation it is possible to build the focusing grating for different value  $h$  of focusing distance. The calculation has been implemented in *Matlab*<sup>®</sup> (Appendix ) for a grating  $4 \mu m$  wide, composed of 30 grooves, and for different value of  $h$  in the range  $[20 \div 100] \mu m$ . The grating so obtained is then exported in order to be read by *L-Edit*, where all the optical setup is designed.

### 3.3 Final Design

Once the optical elements are simulated and correctly designed, the layout of the full structure, with the integration of optical and electrical parts, has been obtained using *L-Edit*. The two parts are designed in two different layers, the bottom one for the optical part and the top one for the electrical one. The two systems will be then fabricated with two different masks that have to be aligned. For the optical part the structures are obtained etching the  $Si_3N_4$ , so since the lithography is an electron beam one and exposes

a positive resist, therefore the layout has to be the negative of the wanted structure. To minimise the exposure time, only a  $2.5\ \mu\text{m}$  wide ridges around the waveguide is exposed, as it is possible to see in figure 3.7. For the electrical part, again electron beam lithography

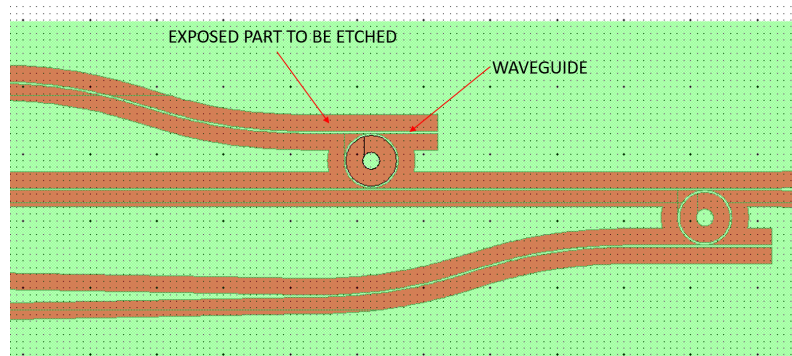


FIGURE 3.7: Zoom on the design of the optical part of the probe. The red areas are the one that will be exposed and after etched.

is used, but the electrodes are obtained through lift-off of a layer of deposited gold, so the areas that will be etched are the one corresponding to the electrodes and pads themselves.

The two systems don't have to interfere one with the other, so since the optical one lies below the electrical one, it is necessary to avoid gold electrodes above an output gratings, otherwise the light emitted would be scattered by the gold itself. As a consequence in the final layout the size of some electrodes has been changed and some wires have been bent in order to be moved away from the output gratings.

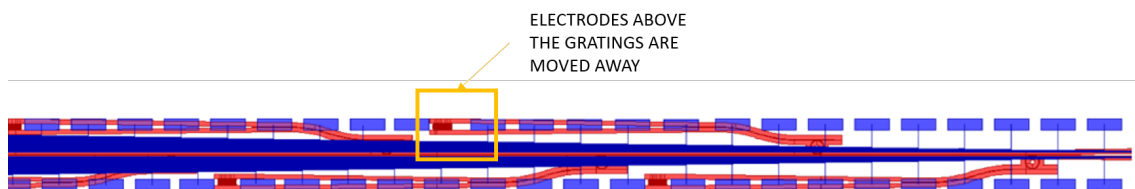


FIGURE 3.8: Design of the overlapping of the optical and electrical layers of the probe. The electrodes over the focusing gratings are moved away

### 3.4 Fabrication process

The starting wafer, depicted in figure 3.9, is a *Lionix TripleX*<sup>[52]</sup>, a commercially available substrate composed by:

- 525  $\mu\text{m}$  thick *Si* layer
- 2.5  $\mu\text{m}$  thick layers of  $\text{SiO}_2$  low pressure chemical vapor deposited (LPCVD), on both side of the *Si* layer
- 160 nm thick layer of  $\text{Si}_3\text{N}_4$  LPCVD, on both the  $\text{SiO}_2$  layers



FIGURE 3.9: Starting wafer, provided by *Lionix*<sup>®</sup>

This substrate is chosen because the LPCVD allows high optical quality and low stress between the layers.

#### 3.4.1 Optical probes fabrication

The first part fabricated is the optical one, which is obtained directly on the  $\text{Si}_3\text{N}_4$  of the *Lionix* wafer. The fabrication exploits electron beam lithography, in order to obtain high resolution during the patterning of the layout. The optical system is designed using *L-Edit*, after the simulation of the structure with *Lumerical*. ZEP 520A, an e-beam positive resist, is then spun on the wafer, exposed and developed in Amyl Acetate.

The ZEP residues are removed with a descum step, i.e. an Oxygen plasma Reactive Ion Etching (RIE) for 30s.

Then RIE with is used to etch the  $\text{Si}_3\text{N}_4$  layer and define the optical circuits. The chemistry used is  $\text{CHF}_3$  and  $\text{O}_2$  in ratio 48:2, for 9 minutes.

After that the ZEP is removed by ultrasonications in dichloromethane, for 10 minutes, and acetone, for other 10 minutes, and then soaking in IPA for 2 minutes.

Finally a 2.5  $\mu\text{m}$  layer of  $\text{SiO}_2$  is deposited with PECVD at 150°C as passivation layer, in order to separate the optical system from the following electrical one.

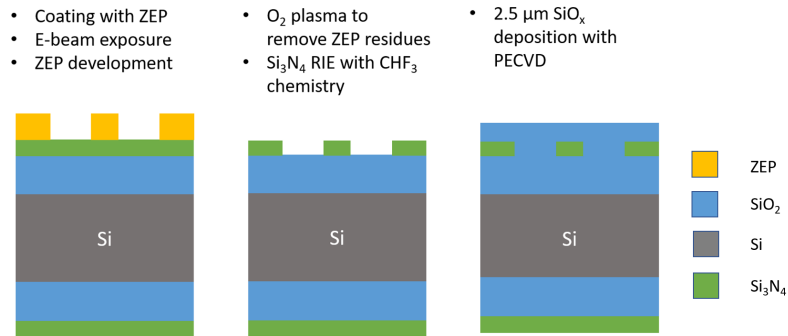


FIGURE 3.10: Fabrication steps for the fabrication of the optical system

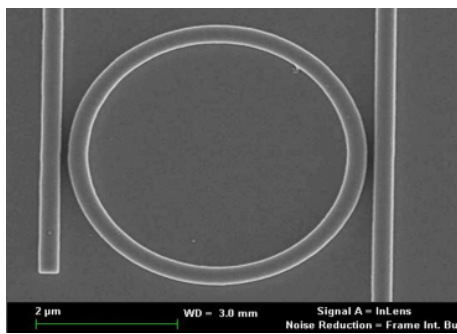


FIGURE 3.11: Ring Resonator

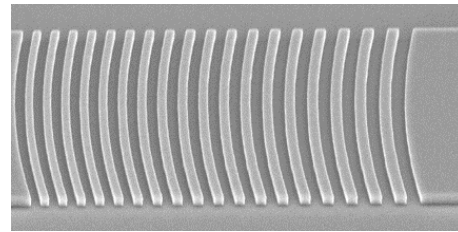


FIGURE 3.12: Zoom on a focusing grating

### 3.4.2 Electrodes and interconnections fabrication

The second part is the fabrication of the electrical circuit. The layout is again drawn using *L-Edit* and it is transferred to the substrate with electron beam lithography.

ZEP 520A is spun on the top face of the wafer and then exposed with the electron beam tool. After it is developed in Amyl Acetate and the residues are removed with a descum step.

After that two steps of electron beam evaporation are performed:

- 10 nm thick layer of Titanium, as adhesion promoter
- 100 nm thick layer of Gold

Then to obtain the desired features, a lift off process is performed, leaving the wafer in Remover-PG at 80° for one hour: the resist is dissolved by this strong solvent, allowing the removal of the gold on the undesired regions. Finally the wafer is cleaned in acetone and IPA.

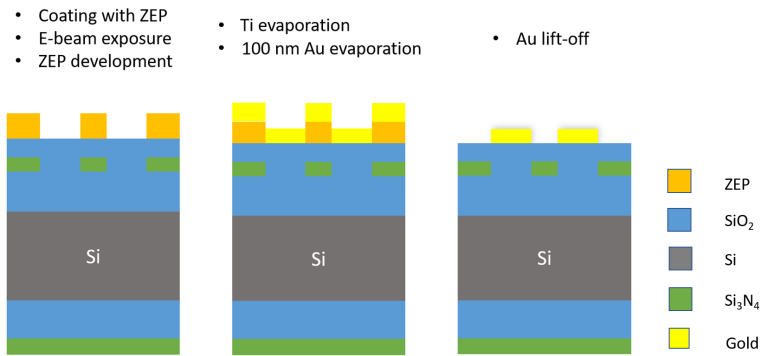


FIGURE 3.13: Fabrication steps of the electrical system

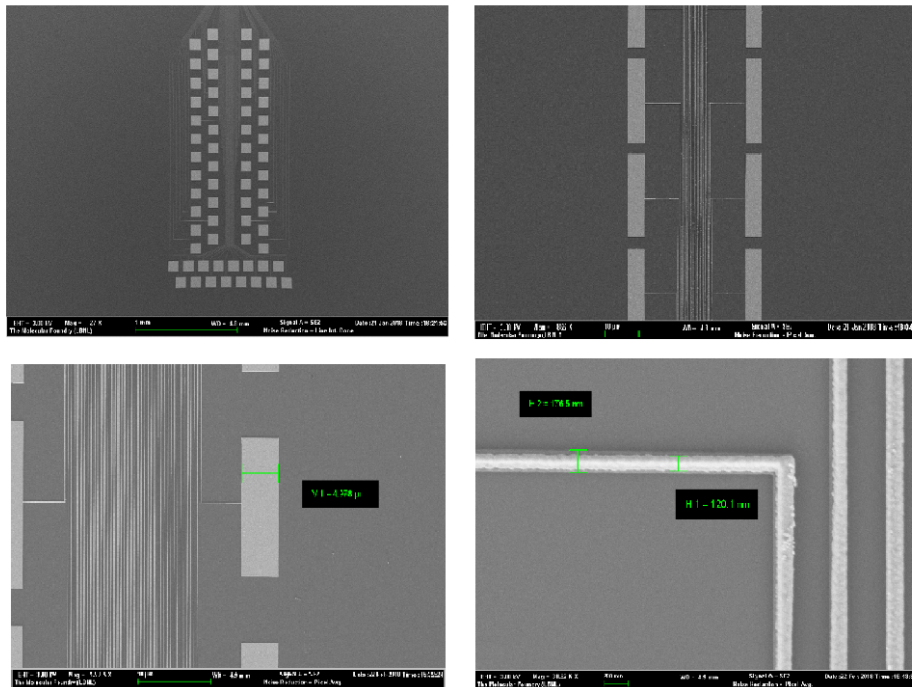


FIGURE 3.14: SEM images of the electrical part of the probe after lift-off

In order to avoid unwanted interactions between wires and neurons, a  $\sim 140 \text{ nm}$  thick passivation layer of  $\text{SiO}_2$  PECVD is deposited on the top side of the wafer. Then another step of electron beam lithography is used to remove the oxide above the electrodes: ZEP is spun and exposed and the  $\text{SiO}_2$  is etched using a  $\text{CHF}_4$  chemistry. After that the ZEP is removed in Remover-PG and the wafer cleaned in acetone and IPA.

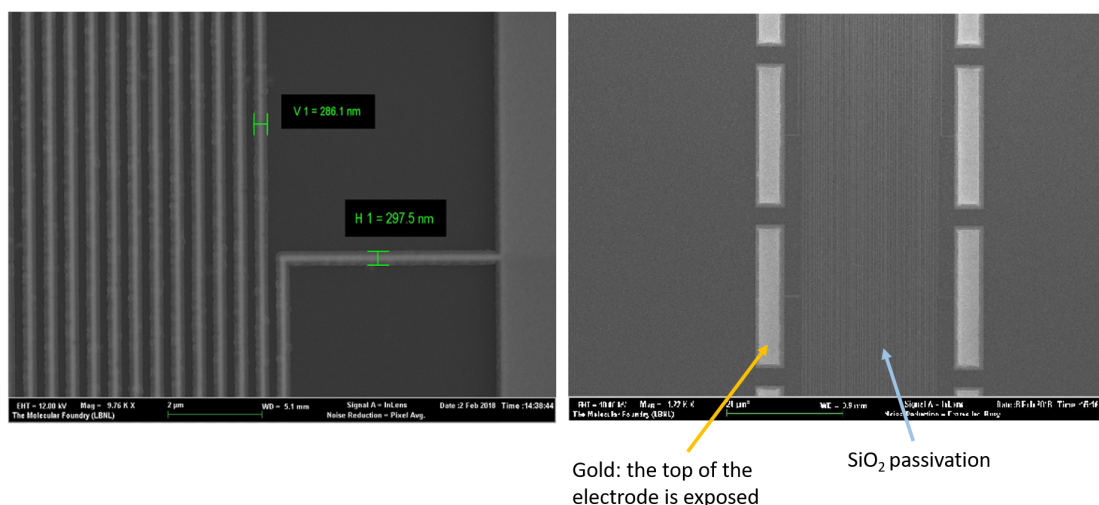


FIGURE 3.15: SEM images of the electrical structure after the passivation. On the left it is possible to see the wire covered by the oxide, while on the right the gold electrodes have been already again exposed, removing the Oxide above them.

### 3.4.3 Etching for shank and support

Once the patterning of the probes is obtained, the wafer is prepared to perform the backside etching needed to thin the shank up to  $20\ \mu\text{m}$ , while leaving the body thicker.

The first step is the electron beam deposition of a 180 nm thick layer of Chromium on the back side of the wafer. The layer is patterned through optical lithography: the adhesion promoter HMDS and positive resist MAP 1215 are spun and then the resist is exposed and developed in a basic solution (MAD 331). The exposed part, i.e. the one under the shank of the probes, are then wet etched in chromium etchant, and so the hard mask for the backside etching is obtained.

The  $\text{Si}_3\text{N}_4$  layer is dry etched in the RIE tool, using a  $\text{CHF}_3/\text{O}_2$  chemistry.

Next step is the etching of most of the Silicon of the shank in KOH, so, in order to protect the frontside wafer during the process, a polymeric layer of PROTEK<sup>[53]</sup> is spun on it, able to withstand KOH for several hours.

The wafer is then immersed in the KOH bath and the areas underneath the shank of the probes are etched away. The etching depth is monitored using a profilometer. Once the thickness is around  $20\ \mu\text{m}$ , the etching is stopped by soaking the wafer in deionized water.

Finally the PROTEK layer is removed in PROTEK removal overnight.

The backside etching is then finished and it is possible to start the frontside etching, which will bring to the release of the probes.

First a 270 nm layer of Chromium is electron beam evaporated on the frontside that will work as mask. Again optical lithography is used to expose the expose MAP 1215 resist previously spun on the wafer. The pattern obtained is a  $100\ \mu\text{m}$  wide trench around the

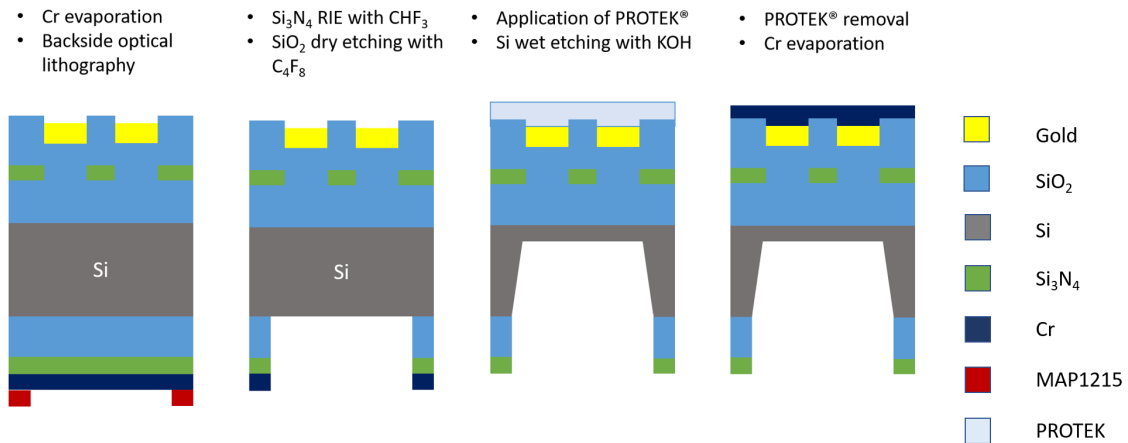


FIGURE 3.16: Fabrication step for the backside etching

probes, that will allow the etching of the borders of the probes and then their release. Chromium layer is then etched in Chromium etchant, defining the hard mask for the frontside.

Another layer of Cr is then electron beam evaporated on the backside, used as a support for the probes during the Si etching and a temperature dissipater during the dry etching at high temperature, avoiding undercut below the probe shanks.

After that the layers of Nitride and Oxide are dry etched in the RIE with  $\text{CF}_4/\text{O}_2$  chemistry, while the Si layer is etched with  $\text{SF}_6$  in an Inductively Coupled Plasma RIE tool, at  $-120^\circ\text{C}$ <sup>[54]</sup>.

In the last step resist is removed with acetone and IPA and the probes are release in chromium etchant.

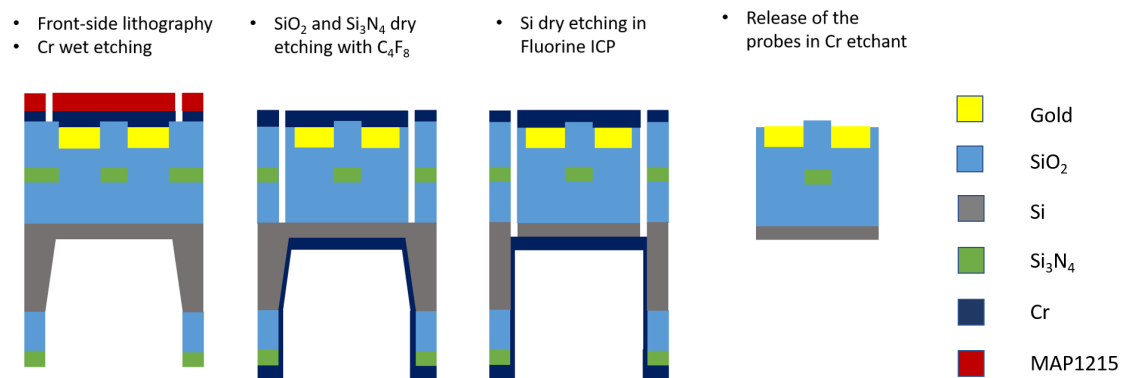


FIGURE 3.17: Fabrication steps for the frontside etching

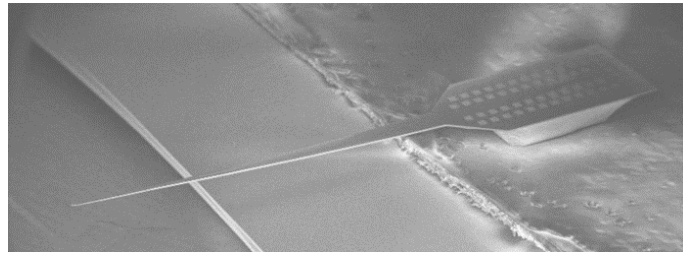


FIGURE 3.18: SEM of a released probe.

*The body of the probe is left thicker for support and handling reasons, while the shank, which will be inserted in the brain, is much thinner*

### SiO<sub>2</sub> Etching Optimization

The first recipe implemented for the etching of the Oxide, able to dig 100  $\mu\text{m}$  wide and 5  $\mu\text{m}$  deep trenches in order to define the shape of the probes, used a  $\text{C}_4\text{F}_8$  gas chemistry at RF=100W. The results of this experiment showed, as depicted in figure 3.19, the formation of a layer of pillars inside the trenches, coming from the Chromium mask which is etched and resputtered in the trenches, as it can be seen from the XPS analysis reported in figure 3.20, where it is possible to see the presence of Cr inside the trenches. These pillars bring to the saturation of the etching itself.

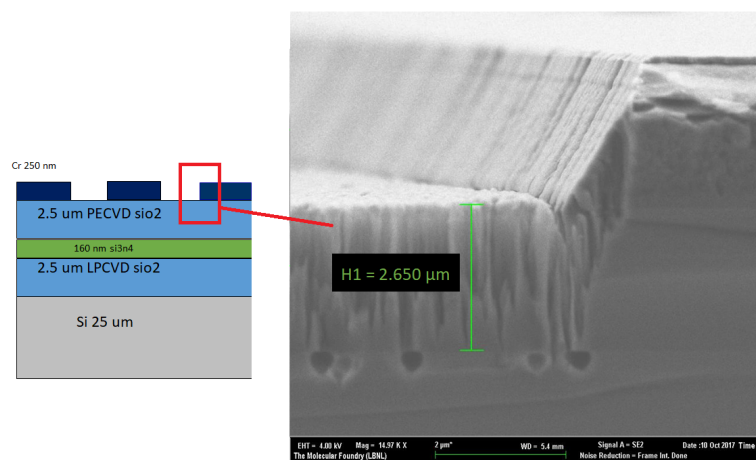


FIGURE 3.19: Formation of pillars inside the trenches which rings to the saturation of the etching

To solve this problem, the first attempt that has been tried was to increase the flow of  $\text{C}_4\text{F}_8$ , from 10 to 40 sccm, and decrease the one of  $\text{O}_2$ , from 40 sccm to 10 sccm. The results of the experiment was good in term of etching, since there was no formation of pillars and the etching went down until the end of the Oxide layer, as it an be seen in figure . At the same time the change on the flows led to the formation of a polymer in the chamber which covered all the walls of the tool, preventing other recipes to be used until the cleaning of the chamber. Then the recipe was not reusable and it was need to find another solution.

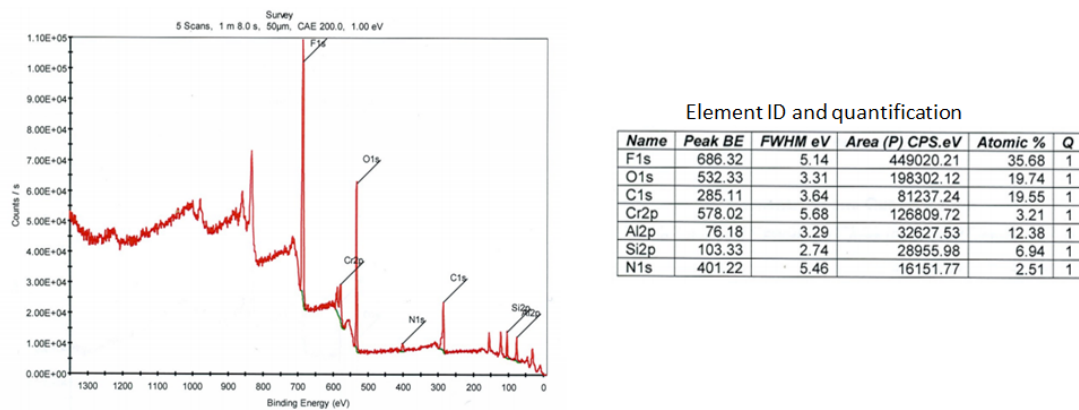


FIGURE 3.20: XPS analysis of the materials inside the trenches after the etching with  $C_4F_8$

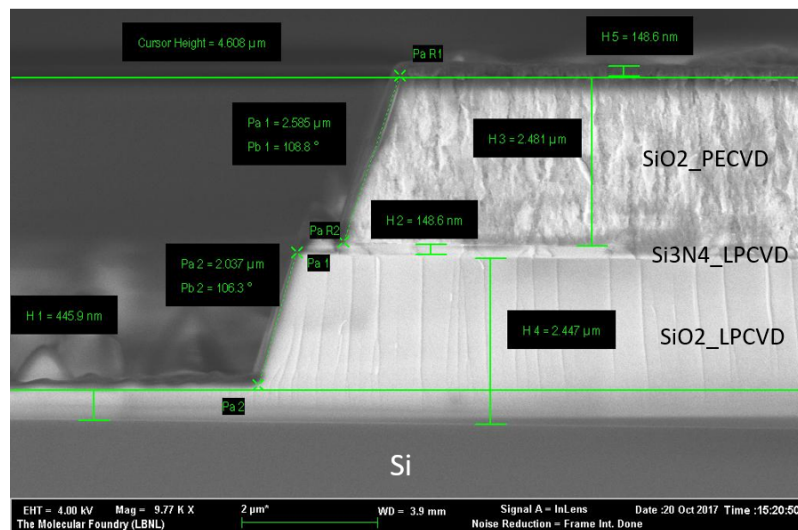


FIGURE 3.21:  $C_4F_8=40$  sccm,  $O_2=10$  sccm  
No formation of pillar

The solution was found in the change of the gas chemistry, from  $C_4F_8/O_2$  to  $CF_4/Ar$ . What can be seen is that there are no more pillars in the trenches and the etching is of the desired height, as shown in figure 3.22.

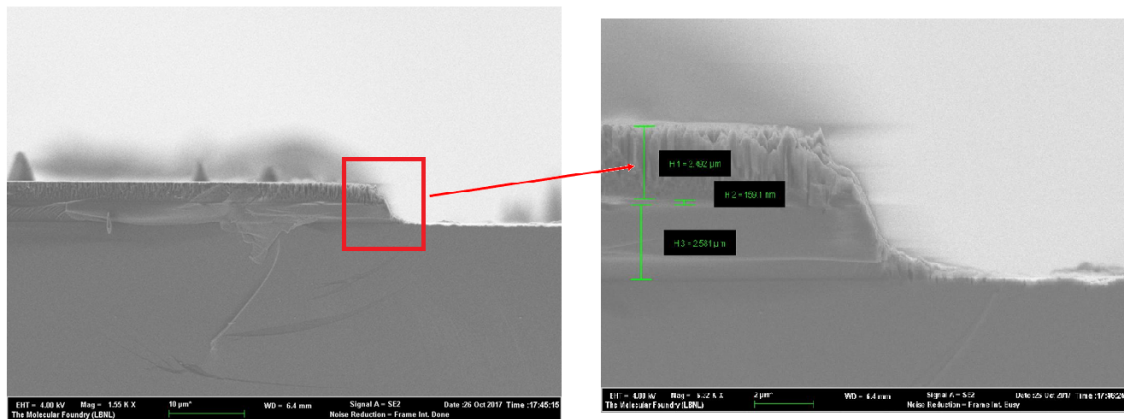


FIGURE 3.22: Etching with  $CF_4$  results  
*The trench is completely etched and there is no formation of pillars*

## Chapter 4

# Graphene integration on the probes electrodes

During the project, beyond the study and development of the general fabrication processes, also the possibility of modify the electrodes surfaces has been investigated. The material chosen to exploit this purpose is graphene. The work involved all the graphene process, from the growth to the transfer of the material on the substrate, i.e. the probes fabricated on the full wafer. Then the study of how it is possible to integrate graphene in a standard nanofabrication process has been examined, achieving an efficiently method to transfer and pattern the graphene, working on wafer-scale dimensions.

### 4.1 Growth of graphene

The integration of graphene on the probes electrodes started with the growth of the material itself. The mostly used method for growing large-scale graphene is Chemical Vapor Deposition (CVD) on metal substrates<sup>[55]</sup>. For this project Plasma-Enhanced CVD at high temperature on Copper foil has been used. This technique allows to deposit thin films from a gas to a solid state on a catalytic substrate. The process involves the creation of a plasma inside the chamber, whose radicals chemically react with the substrate.

A sample of the desired dimensions is cut from the entire roll of Copper foil. In order to make it suitable for the growth, so in particular remove the impurities and the oxide layer that naturally grows on the foil, the sample is pretreated in Acetic Acid for 5 minutes and then rinsed with acetone, for 2 minutes, and water<sup>[56]</sup>. Once dried, the sample is loaded inside the CVD chamber, shown in figure 4.1, and the growth can start.



FIGURE 4.1: Aixtron Black Magic CVD

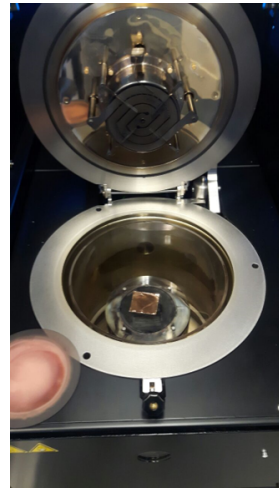
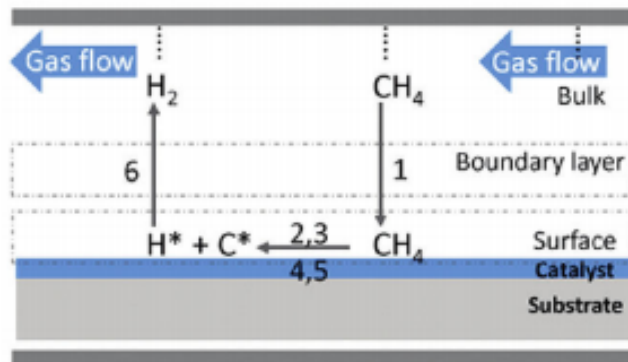


FIGURE 4.2: The sample is put inside the CVD chamber

The process inside the chamber involves the decomposition at high temperature ( $\geq 900^\circ$ ) and low pressure (mbar) of a carbon precursor gas, i.e. Methane. The decomposition of  $CH_4$  produces carbon and hydrocarbon radicals inside the chamber that react with Copper, which acts as a catalytic substrate (fig. 4.3). The reaction make possible

FIGURE 4.3: Schematic of the growth kinetics of graphene on Cu  
*Reprinted from [57]*

the starting of the nucleation of graphene. The full process last for about 2 hours, after which, when the chamber is cooled down to  $\sim 100^\circ C$ , the sample can be pulled out and analysed.

The graphene grown on Copper foil can be initially identify using a standard microscope, with which it is possible to see the formation of the grains on the sample, as depicted in figure 4.4.

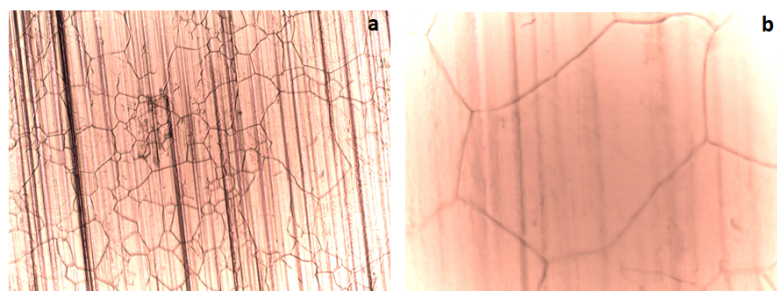


FIGURE 4.4: Graphene grown on Copper Foil, a) with 10x objective b) with 50x objective

### 4.1.1 Raman Spectroscopy of graphene

The tool typically used to analyse graphene samples is Raman Spectroscopy, a powerful technique for studying the geometric structure and the bonding within molecules of a sample in a non invasive way. It is able not only to determine the presence of graphene, but also to give information about its quality and number of layers. A laser beam, at 532 nm wavelength, impinges on the sample under analysis and interacts with molecular vibrations of the material, inducing a shift of the energy of the laser photons. The shift depends on the vibrational modes of the system, and so it gives information about the structure of the material itself. Each material will then have a specific Raman spectrum, whose peaks are related to the molecules which is made up of and their height to the geometric structure.

In the case of graphene, the Raman spectrum exhibits 3 bands:

- G band, around  $1585\text{ cm}^{-1}$
- 2D band, around  $2700\text{ cm}^{-1}$ , usually strong for a highly quality graphene
- D band, around  $1350\text{ cm}^{-1}$ , the defects band

From the intensity of the peaks it is possible to understand the quality of the graphene and the number of layers. Indeed, if the D peak it is really high, this means that the graphene is full of defects. Moreover, to have a monolayer graphene, the intensity of the 2D peak should be twice the one of the G peak, so, depending on how much higher the 2D peak will be respect to the G one, it is possible to have an estimate on the layers of the grown graphene. A typical Raman Spectrum of graphene is the one reported in figure 4.5, where it is possible to see the characteristic peaks. The bell shape base of the spectrum is due to the luminescence of Copper, always there when using a 532 nm laser<sup>[57]</sup>.

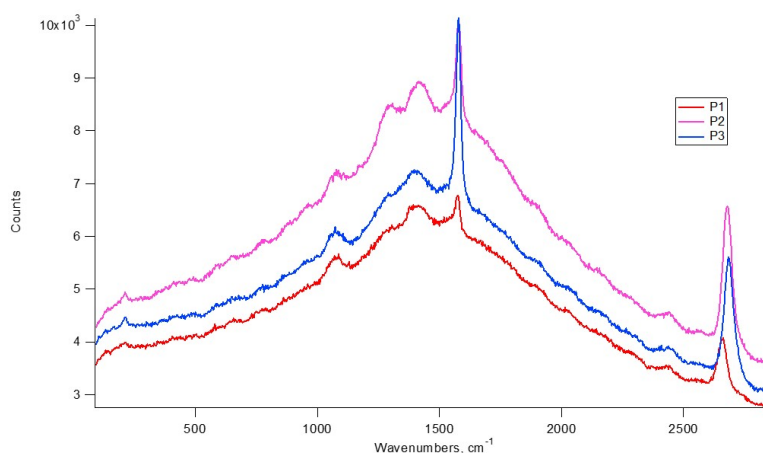


FIGURE 4.5: Raman spectrum of 3 points of a sample of graphene on Copper

### 4.1.2 Graphene growth optimization

To optimize the growth of the graphene changes on the standard recipe have been tried. They involved both the pretreatments on the copper foil itself and the parameters of the recipe.

#### Pretreatments

Typical experiments of graphene growths involved a cleaning of the copper foil through acidic and basic etchants, such as acetic acid, hydrochloric acid or nitric acid<sup>[58]</sup>. The analysis of the effects of these different pretreatments shows how it is possible to obtain better results using Nitric Acid instead of Acetic one, as depicted in figure 4.6.

Therefore the achievement of real better results has been obtained by adding an annealing step before the starting of the growth, obtained with the exposition of the sample in an  $H_2$  plasma atmosphere for at least 30 minutes<sup>[58]</sup> (fig. 4.7). Thanks to the annealing, the copper surface turns from a rough one into a clean and smooth surface. As depicted in figure 4.8 the Raman peaks result to be much more intense in this case.

#### Change in the recipe

In previous publications the effect of different parameters on CVD growth of graphene have been studied, like the pressure, gases flow and growth time<sup>[59,60]</sup>. For this project, instead, the focus has been placed on the variation of temperature<sup>[61]</sup>. In particular the growth has been performed at different process temperatures, starting from 1000 °C, the temperature used in the standard recipe provided by the company of the CVD tool, to 1030°C. For lower value of temperature the nucleation does not start, while for higher one the chamber would approach the melting point of the copper itself. As shown in figure 4.9, the increase of the temperature allows better results: the peaks are more intense and the 2D peak is higher than the G one, which means that the graphene obtained is more

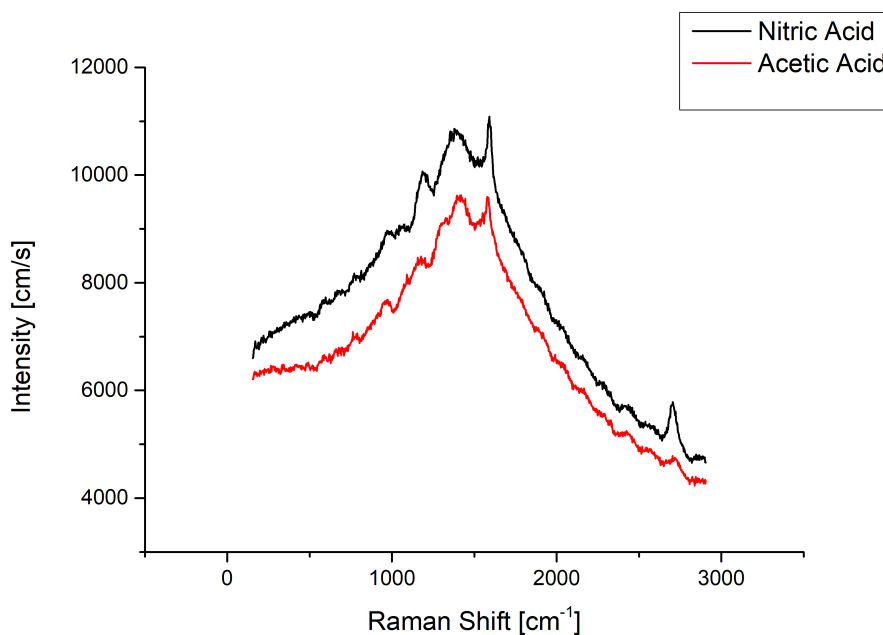


FIGURE 4.6: Comparison between Raman Spectrum of Graphene on Copper foil treated in acetic acid and Copper foil treated in nitric acid

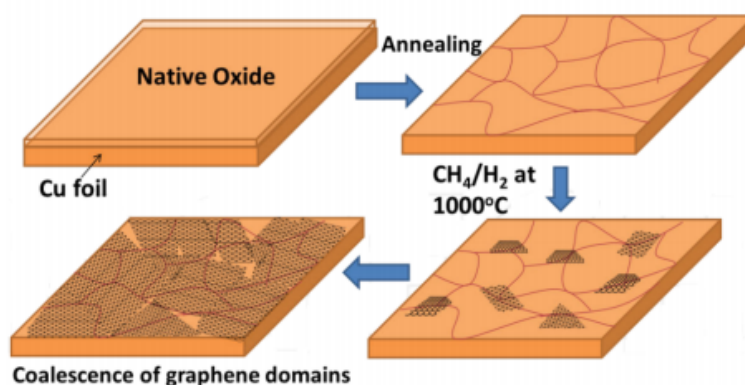


FIGURE 4.7: Graphene growth process

*Amorphous Cu with a native oxide layer is annealed in a hydrogen rich atmosphere at 1000 °C. The hydrogen gas reduces the native oxide layer. In the growth phase methane is introduced in the chamber, starting the nucleation and growth of graphene. Reprinted from [57]*

likely a monolayer one.

At the same time it is not possible to increase too much the temperature, since this can lead to the start of a second nucleation of graphene above the first one<sup>[61]</sup>, and a lower intensity of the peaks, as shown in figure where the growth has been done at 1060°C.

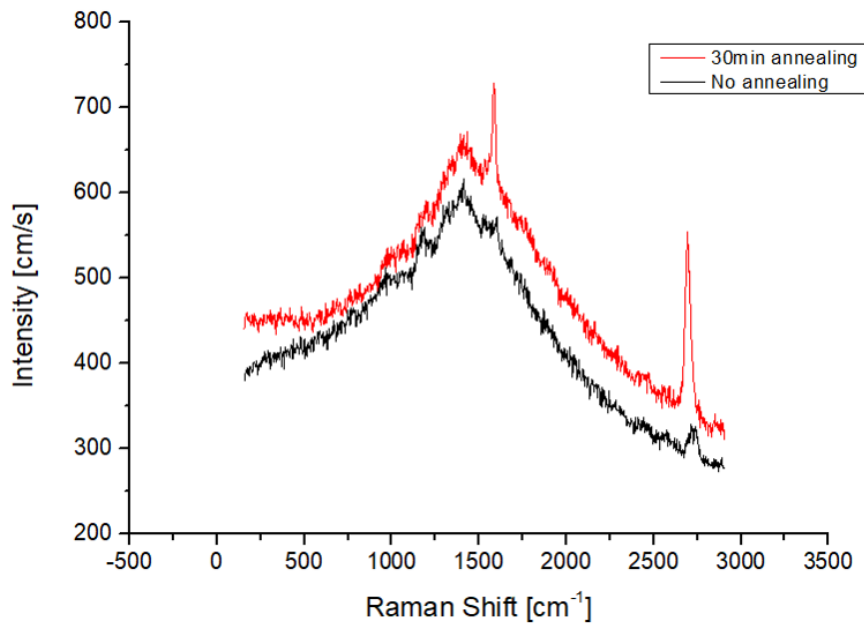


FIGURE 4.8: Comparison between Raman Spectrum of Graphene on Copper foil treated with an annealing step and Copper foil without this pre-treatment

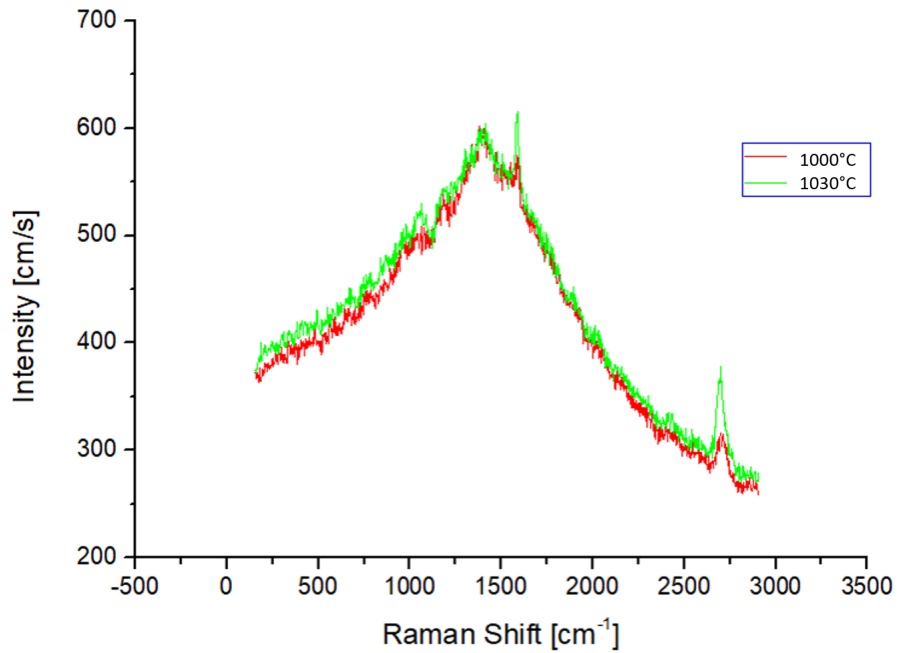


FIGURE 4.9: Raman Spectrum of Graphene on Copper Foil for different growing temperature

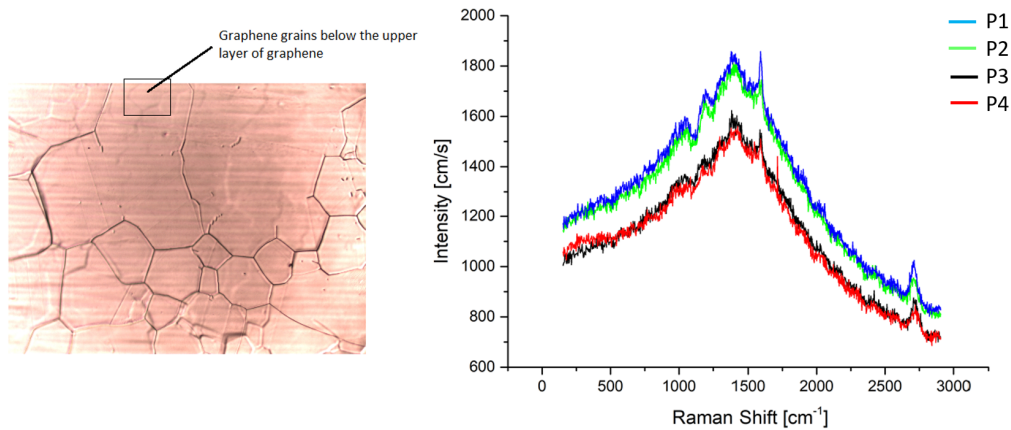


FIGURE 4.10: Effect on the graphene growth for a run performed at 1060°C

## 4.2 Transfer

Once the growth of graphene is optimized, it is possible to start studying the transfer process of the material on the desired substrate. The steps used during this project, all performed inside the cleanroom, are the following one:

1. Firstly a polymer is spinning on the Graphene/Copper sample. The one chosen is a solution of 4% of PMMA in Chlorobenzene, with a molecular weight of 950. With a speed of spinning of 3000 rpm a carrier  $\sim 300$  nm thick is obtained. The sample is then cured in oven at 180°C for 10 minutes.
2. The sample is placed upside down on a clean Si wafer and the backside is wiped with acetone and IPA to remove any residuals of PMMA. Then the sample, always with PMMA side down, is load into the RIE chamber and a 1 minutes  $O_2$  etching at 80 W is used for the removal of the backside graphene
3. The sample is then left floating, with PMMA side up, on Copper etchant ( $FeCl_3$ ) for about 2 hours.
4. Once all the copper foil is etched away, the left graphene/PMMA sample is transfer, with the help of a Si wafer piece, to clean DI water and left float for about 10 minutes. Then the sample is transfer to other clean DI water and let sit for about 1 hour.
5. After the rinse in water, which allows the graphene to be cleaned from any copper etchant residuals, the sample is lift off onto the target substrate and let sit vertical to dry for 1 hour.
6. When the sample is completely dried it is possible to remove the PMMA carrier in a solvent. It is then left soaking in acetone for 2 hours, after which it is rinsed with IPA and blown with  $N_2$

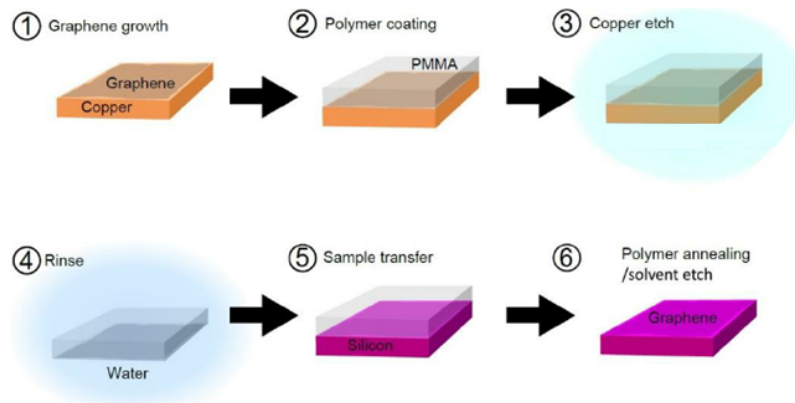


FIGURE 4.11: Transfer process of the graphene on the desired substrate

### 4.2.1 Transfer of graphene on gold

Since the graphene on the probes has to be integrated on the top of gold electrodes, the adhesion of graphene on gold has been tested, transferring a layer of graphene on a wafer covered by an evaporated layer of gold. The Raman results after the transfer, depicted in figure 4.12, show that the graphene has been correctly transferred onto the gold substrate, proving the good adhesion between the two materials.

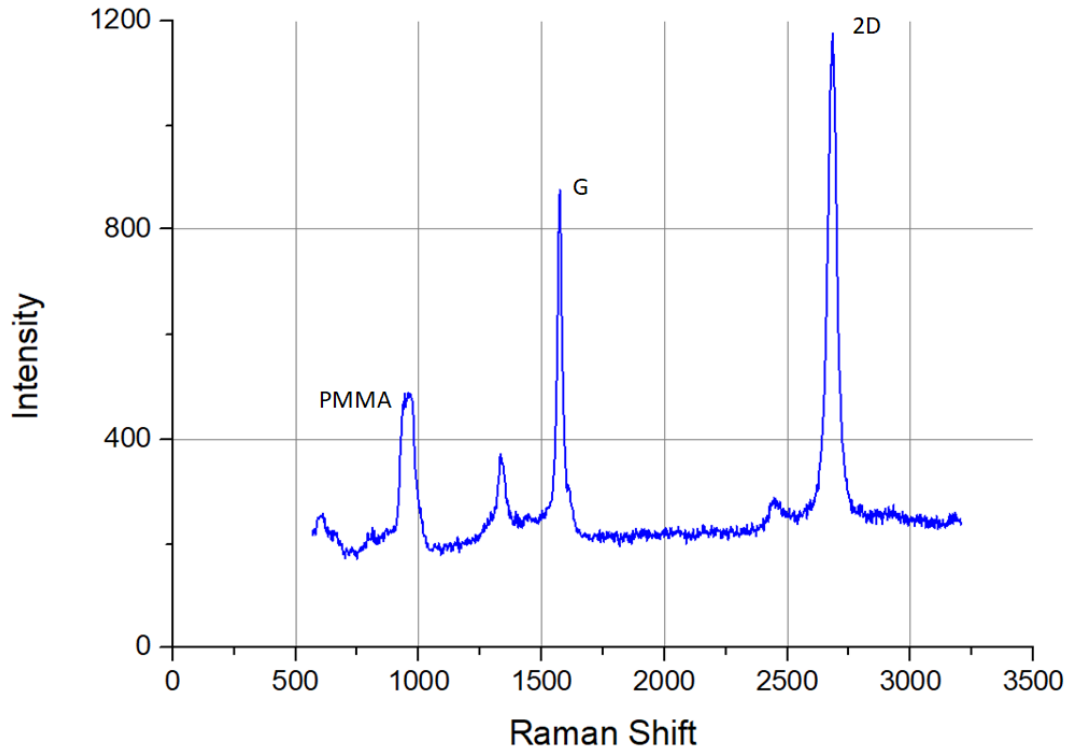


FIGURE 4.12: Raman Spectrum of graphene transferred on a gold substrate

Thus graphene has been transferred onto the target substrate, i.e. the wafer with the probes. Some pictures of the transfer process performed inside the cleanroom are shown in figure 4.13.

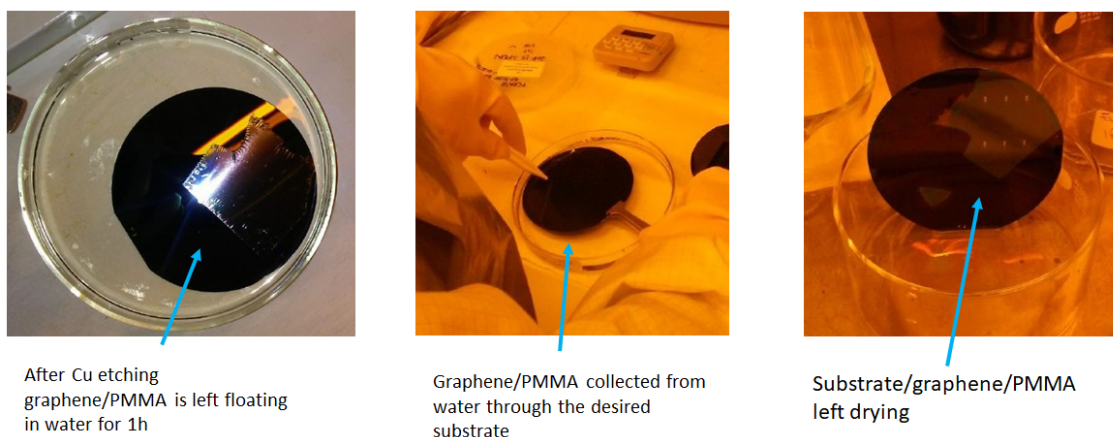


FIGURE 4.13: Transfer of graphene sample on a wafer with the final probes

The results of the transfer are shown in figure 4.14, which represent the SEM images of the shank of a probe: the uniformity of the graphene is enough good to cover all the gold pads. Even if the sample has been left for 2 hours in acetone, there are still residuals of PMMA.

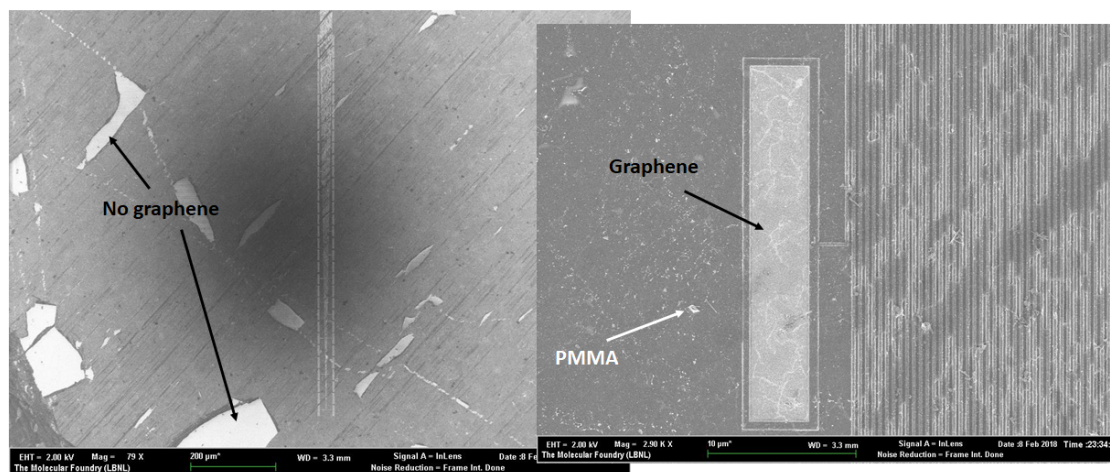


FIGURE 4.14: SEM images of the shank of a probe after the transfer of graphene above it

### 4.3 Integration of graphene on the pads

Once the graphene has been transferred on the wafer with the probes, it is necessary to pattern it, in order to have only the gold pads, i.e. the features which will be in contact

with the neurons, covered with the graphene.

Thus the integration of the graphene is inserted in the fabrication process after the  $SiO_2$  passivation of the wires and the aperture of the gold electrodes.

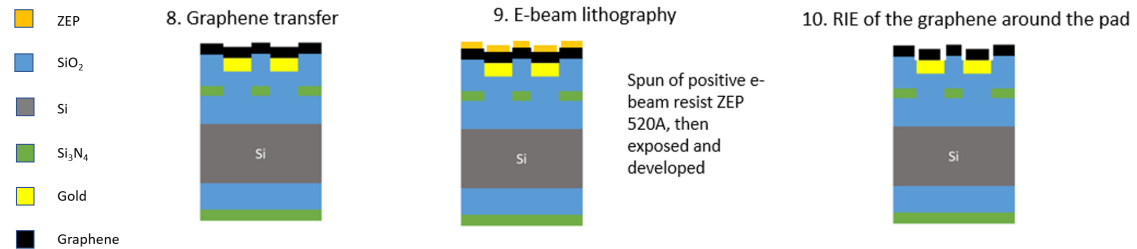


FIGURE 4.15: Fabrication steps for the patterning of graphene

Once the full graphene layer cover the wafer, the defining of the shape of the electrodes is again obtained with electron beam lithography. This choice avoid the use of lift off, which is a fast and easy way to remove wide areas of materials but in the case of graphene could cause the peel off of the whole graphene layer. At the same time, since the electron beam exposure can not involve all the wafer sized graphene layer, since it would be too expensive in terms of time, it is necessary to choose a CAD layout able to create the electrodes but in a short time: thus the pattern chosen, reported in figure 4.16, expose  $0.5 \div 1 \mu m$  thick trenches around the electrodes. In this way it is possible to define the shape of the pads, which will be no more short circuited, but the material exposed, and then etched away, is the minimum needed for the purpose. The remaining graphene on the probes will not interfere with the other features since the layer of  $SiO_2$  efficiently isolates them.

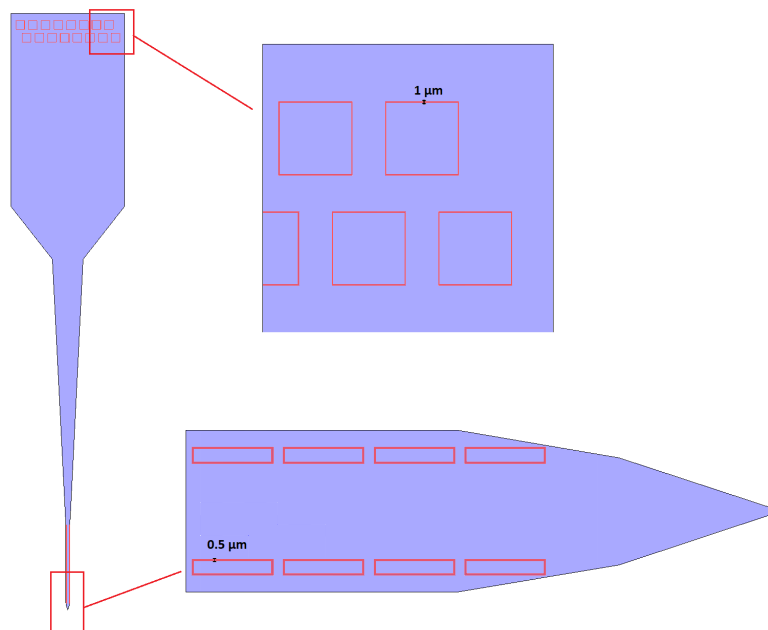


FIGURE 4.16: Layout for the patterning of graphene

Thus ZEP is spun on the graphene layer, with the same recipe of the previous fabrication steps, and then expose with the electron beam tool. After the development of the resist in Amyl Acetate, the wafer is loaded in the RIE and the graphene is etched with  $O_2$  for 2 minutes at 80 W. Finally ZEP is removed in Remover-PG and the wafer cleaned in acetone and IPA.

The sample has been then analysed with the SEM (fig. 4.17): the etching of the trench around the pad efficiently worked.

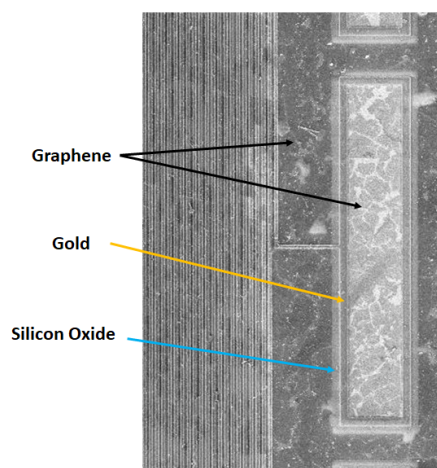


FIGURE 4.17: SEM image of a graphene/gold pad, after the lithography of graphene.

Finally to verify the presence of the graphene on the pads, they have been studied also with the Raman tool. The results are depicted in figure 4.18 and demonstrate that the graphene is correctly transferred on the pads.

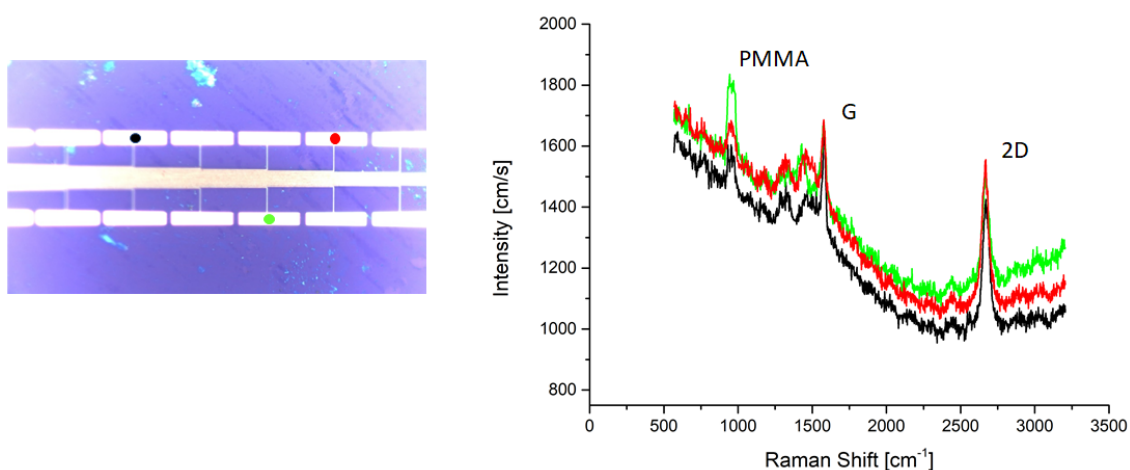


FIGURE 4.18: Raman spectrum on the shank pads: the graphene has been correctly transferred

## Chapter 5

# Measurements and results

Both the optical and electrical parts of the probes have been characterised. In this chapter the measurements setups and the results are presented.

### 5.1 Optical alignment and characterization

The setup used to characterised the optical part of the probe, depicted in figure 5.1, is composed of the following elements:

- a UV laser (wavelength at 405 nm) and a blue laser (wavelength in the range 448 ÷ 452 nm) are coupled to a single mode optical fiber (*Thorlabs - 460HP Single Mode Fibre*), which in turn is coupled to the input waveguide of the probe
- the probe is glued to the PCB, which is, in turn, fixed to a stage placed under an optical objective
- the fiber is glued to a 3D printed stage, moved with micromanipulators too
- a CCD is plugged to the objective and connected to the computer, in order to easily monitor the intensity of the outputs

The optical characterization starts with the connection of the input waveguide to the fiber: thanks to the help of the micromanipulators, the fiber is moved close to the input of the probe (fig. 5.2). The blue laser is turned on and through the CCD the outputs of the structure are analysed: when the intensity of the output spot is maximised the alignment is reached. Once happened, the fiber and the input of the probe are glued together using a UV curable glue: the blue laser is turned off, while the UV one is turned on. The curing time is fast, less than 10 seconds, in order to minimise the risk of misalignment. Finally the backward of the fiber is stuck to the upper part of the PCB with a UV curable glue, in order to avoid further movements of the fiber.

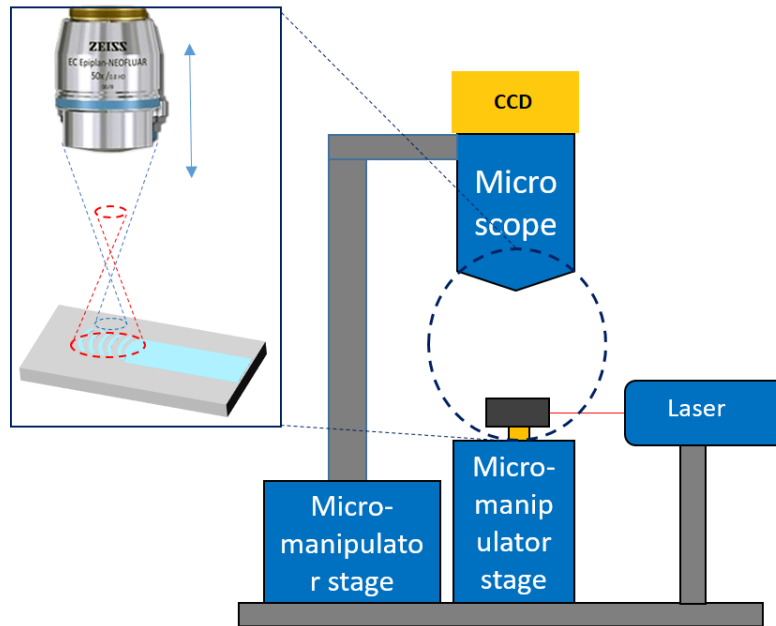


FIGURE 5.1: Optical setup scheme used to characterise the optical structure on the probe.

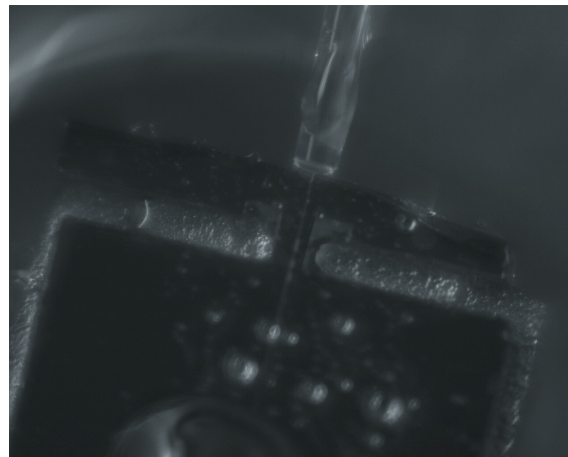


FIGURE 5.2: Once the alignment is reached, the fiber is glued to the input waveguide

### 5.1.1 Optical Characterisation Results

Once the alignment is reached, through the CCD it is also possible to analyse the different optical features designed for the probe.

The correct behaviour of the ring resonators is tested just changing the temperature of the laser, which implies a change on its wavelength: different rings are then selected along the structure as the wavelength of the laser changes with the temperature, as it can be seen in figure 5.3.

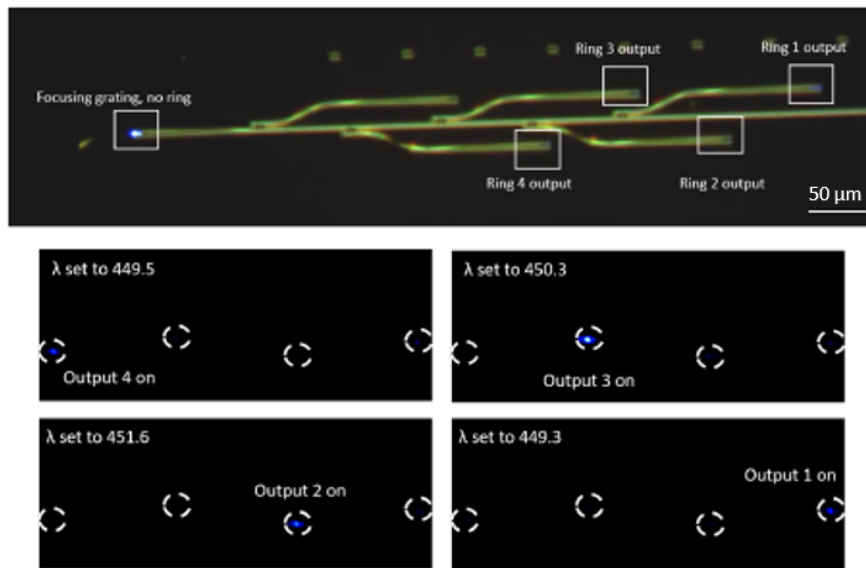


FIGURE 5.3: Images taken from the CCD: (a) Full structure illuminated with white light. (b) Changing the input wavelength of the laser, different rings are selected along the optical structure.

Then also the focusing gratings are analysed, in order to verify if the grating focuses the light at the correct height. The CCD is focused on the surface of the input waveguide, in order to set the 0 level. Then the camera is moved over the outputs, i.e. on the focusing grating, and then is raised along the  $z$  direction from 0 to  $100 \mu m$ , examining the dimensions and the light intensity of the spots at the different heights. The distance at which the output is focused is the height at which the grating focuses the light.

For a better analysis of the outputs, each picture of the spot at different height is analysed with *Imagej*, a software able to return the intensity plot of a selected line. Then selecting a line that crosses the output spot of the grating, it is possible to compare the intensity of the spots at different heights. The results are shown in figure 5.4 and 5.5, where it is possible to see that for a grating designed for focusing the light at a distance of  $20 \mu m$ , around that value the spot is much more clear and intense.

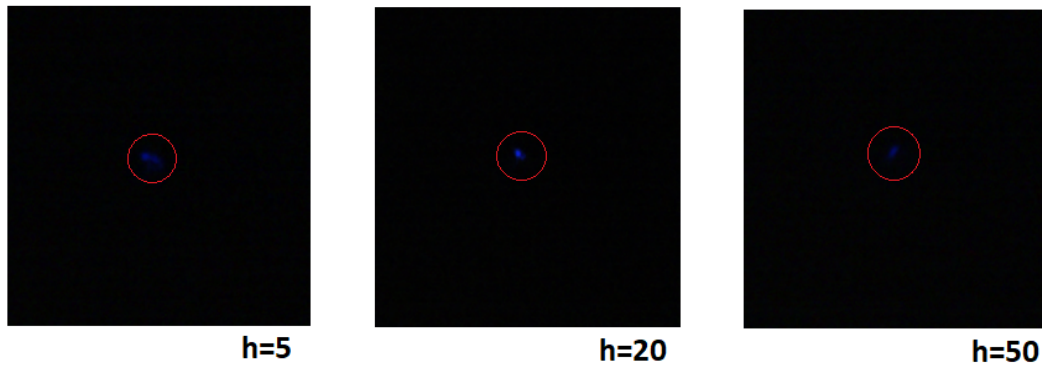


FIGURE 5.4: Pictures of the output spot of a h20 focusing grating, taken at height a)  $5 \mu\text{m}$ , b)  $20 \mu\text{m}$ , c)  $50 \mu\text{m}$

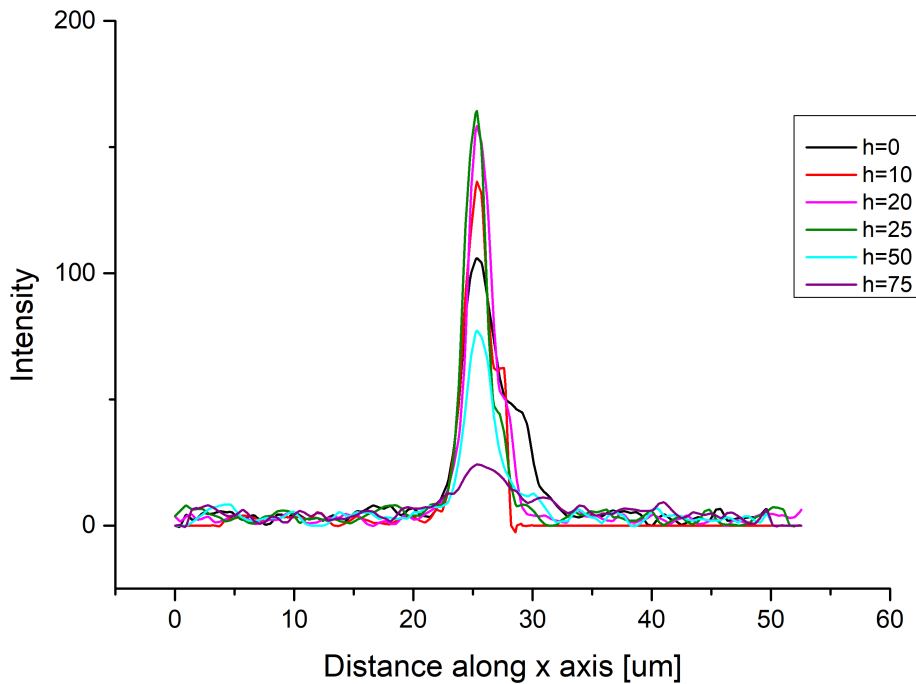


FIGURE 5.5: Intensity plots of the output spot of a h20 grating, obtained from pictures taken at different heights from the feature itself

## 5.2 Electrical characterization of the electrodes with and without graphene

In order to test the electrical circuit, the probe is first glued to a printed circuit boards (PCB). The PCB works both as a handling support and as access to the electrical signals. Indeed it is provided with a series of 64 pads that can be wirebonded to the 64 electrodes

on the top of the probe (fig. 5.6). These pads are connected through traces to an equivalent

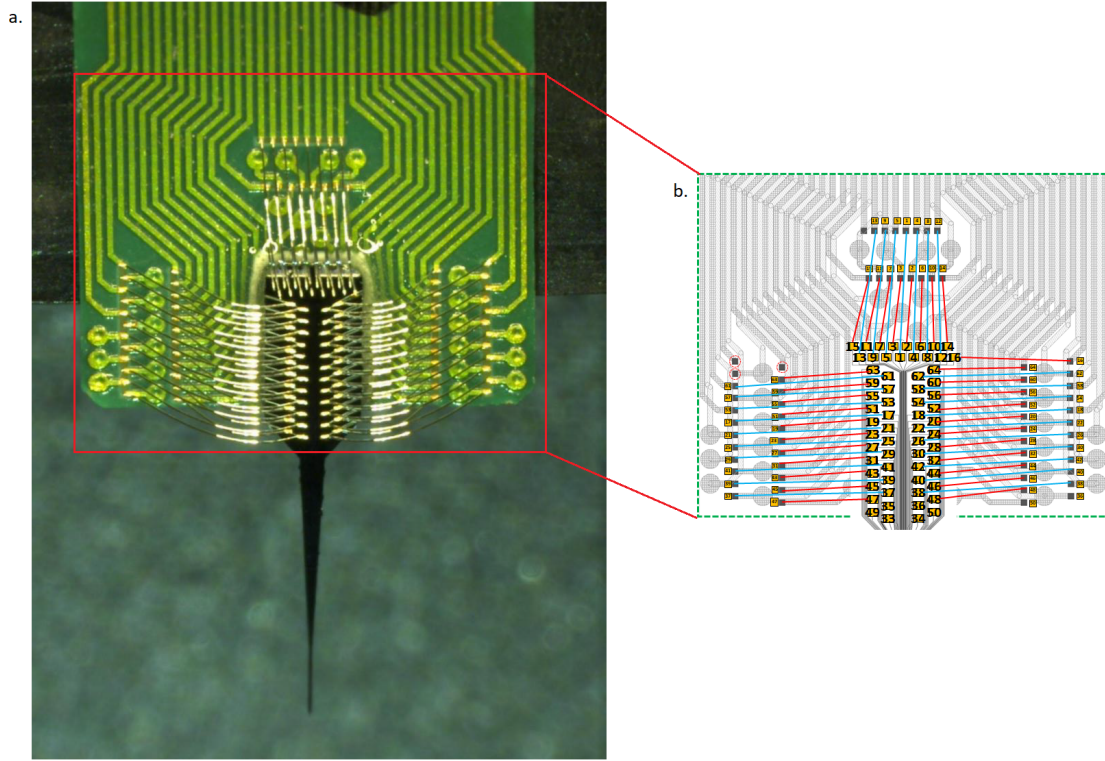


FIGURE 5.6: (a) Wire bonded probe on a PCB. (b) Design of a PCB: zoom on the wire bonding part. Each probe pad can be connected to a single pad on the PCB.

set of 64 pads on the upper part of the PCB, which in turn host Samtec connectors that can be easily plugged in the experimental setup. The instrument used for the impedance measurements is called *NanoZ*<sup>[62]</sup>, a measurement apparatus able to test impedance at different frequencies with small sinusoidal signals. For the measures, the tip of the probe is immersed in a saline conductive saline, while the connectors of the PCB are plugged into the *NanoZ*. The ground is obtained immersing the end of a wire connected to the PCB in the saline solution too.

### 5.2.1 Impedance measurements of the electrodes without graphene

The electrodes have been studied at 200 Hz and 1000 Hz, typical working frequencies of the neurons<sup>[63]</sup>. The average impedances obtained are

$$Z = 4.9 \pm 0.3 \text{ M}\Omega @1000 \text{ Hz} \quad (5.1)$$

$$Z = 64 \pm 9 \text{ M}\Omega @200 \text{ Hz} \quad (5.2)$$

The result is consisted with the one found in literature, as reported for example by Chen et al. in [64], where they studied a probe which hosted gold microelectrode with a radius

of  $16 \mu m$ , finding as impedance values the one reported in figure 5.7.

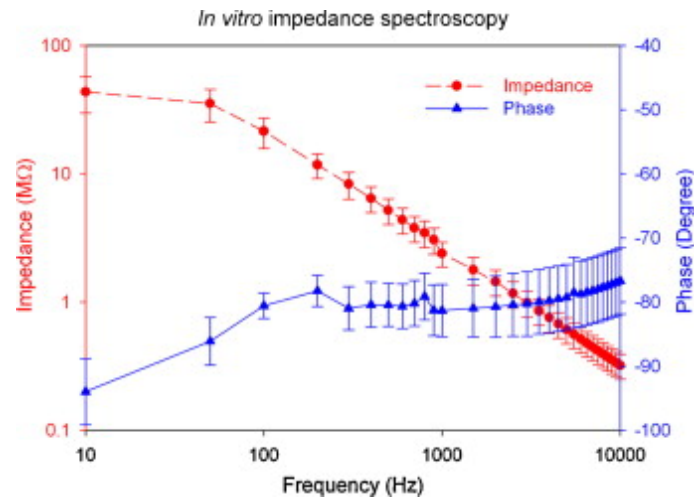


FIGURE 5.7: Impedance spectroscopy of Chen et al. probe, with the impedance spectrum and the phase spectrum ranging from 10 Hz to 10 kHz. The average impedance was  $2.40 M\Omega \pm 0.52 M\Omega$  at 1 kHz.

*Reprinted from [64]*

These values are enough to determine the working of the electrodes, but are not sufficient to record action potentials, which generally have amplitude of tens of  $\mu V$  and so they need low electrode impedance to have a better signal to noise ratio<sup>[65]</sup>.

To solve this problem electroplating is used, a process able to deposit metal atoms on the surface of the electrodes by passing a current through an electrolyte. What obtained is a rough surface of the electrode that provides a wider contact area without changing the dimensions of the electrode itself. The electroplating is obtaining still using the *NanoZ*, changing the saline solution with a Gold Electroplating solution, and applying negative currents in a range from  $-0.1$  to  $-1 \mu A$ . The SEM results of the electroplating are shown in figure 5.8.

The so obtained electrodes are then tested again with the measurements tool. The average impedance is lowered of one order of magnitude, reaching a value much more suitable to analyse neural signals:

$$Z = 482 \pm 163 k\Omega @ 1000 \text{ Hz, after plating} \quad (5.3)$$

$$Z = 1.78 \pm 0.6 M\Omega @ 200 \text{ Hz, after plating} \quad (5.4)$$

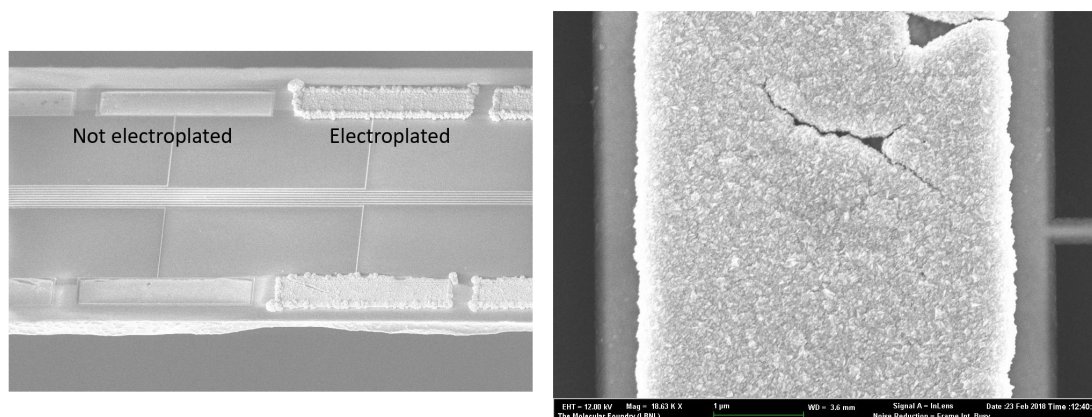


FIGURE 5.8: SEM images of electroplated electrodes

### 5.2.2 Impedance measurements of the electrodes with graphene

Also the gold electrodes coated with graphene have been analysed with the *NanoZ* tool. The average impedance obtained are

$$Z = 2.25 \pm 0.4 \text{ M}\Omega @ 1000 \text{ Hz} \quad (5.5)$$

$$Z = 14.3 \pm 0.7 \text{ M}\Omega @ 200 \text{ Hz} \quad (5.6)$$

The results shown a good electrical properties of the graphene/gold electrodes: the impedance is comparable to the one of the gold electrodes not electroplated, which means that the transfer process of the graphene, even if it is a bit tricky and dirty, does not ruin the properties of the electrodes. Moreover the average impedances obtained are even lower than the gold one, as it is possible to see from the comparison in figures 5.9 and 5.10, even if they remain higher than 1  $M\Omega$ .

A further optimization can be the transfer of graphene on already electroplated gold electrodes, in order to combine the good electrical properties of the graphene and its better adhesion with the neurons with the increase of the contact surface, thanks to the creation of the nanostructures due to the electroplating.

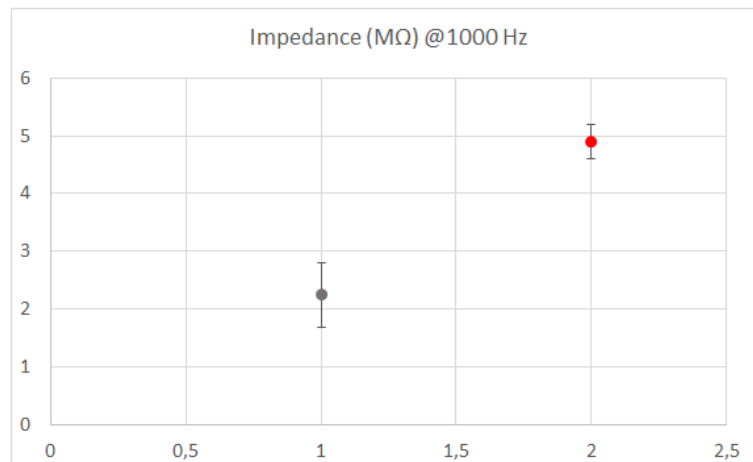


FIGURE 5.9: Comparison of the average impedance of electrodes with and without graphene @1000 Hz

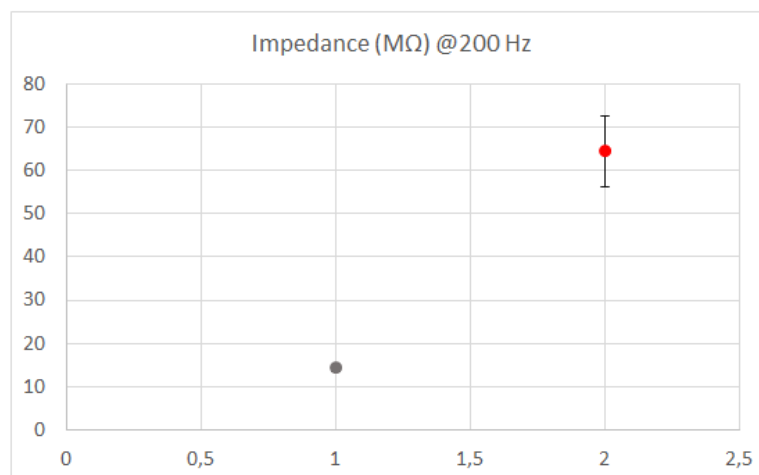


FIGURE 5.10: Comparison of the average impedance of electrodes with and without graphene @200 Hz

### 5.2.3 In Vivo Experiments

Some in vivo experiments have been already performed using the gold electrical probes. The devices are brought to the neuroscientists, who test them on mice. The mouse is prepared with a craniotomy, performed under a microscope: a little hole is drilled in the animal's skull and the probe is implanted and forced to penetrate the dura mater, i.e. the outer layer of the brain. Then, using a micromanipulator, the tip of the probe is inserted to a depth of about  $1000 \mu\text{m}$  in the mice cortex.

The neurons electrical signals collected show the firing of different action potentials, recognizing from the presence of spikes in the signal. Each spike can be after assigned to

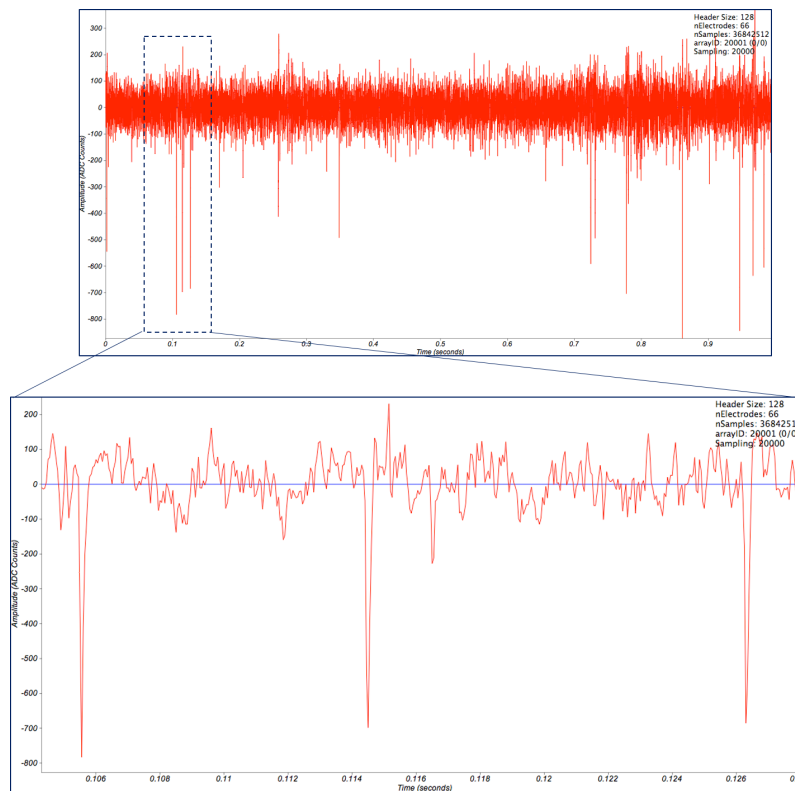


FIGURE 5.11: Electrical signal collected from an electrode. The spikes correspond to the firing of an action potential  
*Provided by Shinya Ito UCSC*

a neuron in a specific position, leading to the possibility of study how the propagation of the signal among the brain. Once the neurons are sorted, studying the shape and the duration of the spike it is possible to achieve knowledge also about the kind of neuron interfered by the probe.

## Chapter 6

# Conclusions

The work here presented described the design, fabrication and characterisation of a multifunctional neural probe. The integration of both an electrical and an optical part on the same device is achieved, allowing the possibility of stimulate the brain with light and record the neurons response in real time. Thus the project will contribute to helping the neuroscientists in acquiring a deeper knowledge on the mechanisms which rule the brain and the communications between neurons.

Further development in the integration of graphene on the electrodes probe have been achieved too, providing new methods to decrease the electrodes impedance and improve the biocompatibility of the device.

### 6.1 Improvement obtained

During the internship several results have been obtained.

Regarding the fabrication process, the steps have been well established and the issues regarding the etching of the frontside of the wafer have been successfully solved: changing the gas chemistry of the etching recipe the Silicon Oxide layer is now etched as expected.

The optical part of the probe has been characterised, studying in particular the focusing capability of the gratings, i.e. the outputs of the optical structure designed on the probe, showing that the experimental results reflect the theoretical one designed with the CAD tool.

Finally the work performed with the graphene has given great results. The growth of the material has been studied from scratch, yielding promising results in a short period. The transfer on the full wafer has been successfully performed, as well as the patterning of the shape of the electrodes exploiting electron beam lithography. During the project it has been thus possible to solve simultaneously different typical issues regarding graphene: the growth and transfer of large area graphene have been done, as well as the patterning of a full wafer coated with graphene, fabricating microelectrodes with dimensions much smaller than the ones usually exploited in literature. This also allowed a direct

comparison between standard gold electrodes and coated gold electrodes, being available the two kind electrodes, with the same geometrical shape but the material changed. The impedance measurements performed in PBS of the electrodes have shown that the graphene coating reduces the impedance of the gold electrode, even if without reaching an impedance value low enough to easily read the action potential signals. Though, this result allows to go on working on this material as a promising coating for microelectrodes, with the support of a well-established growth, transfer and patterning process in a really small shape and in a large-scale production.

## 6.2 Future works

Future work will be focused on optimizing the integration of both the electrical and optical part of the probe, performing in particular *in vivo* experiments of stimulation and recording using these probes. Further it will be possible to start the study of the integration of microfluidic channels on the probe, enabling drug delivery in the brain.

Regarding the coating with graphene, the transfer of the material on gold electroplated electrodes will be tested in order to try to combine both the advantages of the electroplating, increasing the contact electrode area and then decreasing the impedance, and of the graphene, with advantages in biocompatibility and enhancement of the adhesion between neuron and device.

# Appendix

## .1 Matlab implementation of the focusing grating

```

breaklines
1  close all
2  clear all
3  clc
4
5  %SETTINGS
6  %optical parameters
7  lambda = 0.45;           %lambda
8  n_m = 1;                 %refractive index of the medium
9  n_eff = 1.85;           %refractive index of the grating (lower than the one of the wg)
10 %geometrical parameters
11 h = 20;                  %focal distance (um)
12 n_gr = 30;              %number of groves; use even number
13 R = 0.001;              %grid (um)
14 wg = 4;                  %grating width (um)
15 format long g
16
17 pitch = lambda/n_eff;
18 n_y = wg/R+1;
19 punti = zeros (n_gr, n_y);
20 m_center = round(h*n_m/(lambda));
21 m_min = m_center - n_gr/2;
22 m_max = m_center + n_gr/2;
23 m = linspace(m_min, m_max, n_gr+1);
24
25 punti=zeros(n_gr,n_y);
26 for j = 1 : n_y
27     y= (j-n_y/2)*R;
28
29     for i = 1 : n_gr
30         b = n_eff*m(i)*lambda;
31         a = n_eff^2-n_m^2;
32         c = m(i)^2*lambda^2-n_m^2*(h^2+y^2);
33
34         punti(i,j) = (b-sqrt(b^2-a*c))/a;
35     end
36 end
37
38 poligono = [punti; punti+lambda/(2*n_eff)];
39
40

```

```

41 figure
42 hold on
43 for i = 1 : 2*n_gr
44     plot(poligono(i,:), '*')
45
46 end
47
48
49 % figure
50 % hold on
51 % axis off
52 fid=fopen('Focusing_grating3.cif','wt');
53 fprintf(fid, 'DS 1 2 40;\n9 prova85;\nL 2;\n');
54
55 for j = 1 : (n_gr)
56
57     for i = 1 : (n_y-1)
58
59         a = poligono(j,i);
60         b = poligono(j,i+1);
61         c = poligono(j+n_gr,i+1);
62         d = poligono(j+n_gr,i);
63         e = (i*n_y)/n_y;
64         f = e+1;
65
66
67         ab=[2*e,2000*d,2*f,2000*c,2*f,2000*b,2*e,2000*a];
68         abb=round(ab);
69
70         fprintf(fid, 'P %g %g %g %g %g %g %g %g; \n', [abb]');
71
72
73
74     end
75
76 end
77
78 fprintf(fid, '\nDF;\nE\n');
79 fclose(fid);true

```

# Bibliography

- [1] Zoltan Fekete. "Recent advances in silicon-based neural microelectrodes and microsystems: a review". In: *Sensors and Actuators B: Chemical* 215 (2015), pp. 300–315.
- [2] Christopher AR Chapman, Noah Goshi, and Erkin Seker. "Multifunctional Neural Interfaces for Closed-Loop Control of Neural Activity". In: *Advanced Functional Materials* (2017).
- [3] Mohamad HajjHassan, Vamsy Chodavarapu, and Sam Musallam. "NeuroMEMS: neural probe microtechnologies". In: *Sensors* 8.10 (2008), pp. 6704–6726.
- [4] Peter Norlin et al. "A 32-site neural recording probe fabricated by DRIE of SOI substrates". In: *Journal of Micromechanics and Microengineering* 12.4 (2002), p. 414.
- [5] Neil Joye, Alexandre Schmid, and Yusuf Leblebici. "Electrical modeling of the cell-electrode interface for recording neural activity from high-density microelectrode arrays". In: *Neurocomputing* 73.1 (2009), pp. 250–259.
- [6] Robert C Gesteland et al. "Comments on microelectrodes". In: *Proceedings of the IRE* 47.11 (1959), pp. 1856–1862.
- [7] Kip A Ludwig et al. "Chronic neural recordings using silicon microelectrode arrays electrochemically deposited with a poly (3,4-ethylenedioxythiophene)(PEDOT) film". In: *Journal of neural engineering* 3.1 (2006), p. 59.
- [8] Gytis Baranauskas et al. "Carbon nanotube composite coating of neural microelectrodes preferentially improves the multiunit signal-to-noise ratio". In: *Journal of neural engineering* 8.6 (2011), p. 066013.
- [9] Mehdi Jorfi et al. "Progress towards biocompatible intracortical microelectrodes for neural interfacing applications". In: *Journal of neural engineering* 12.1 (2014), p. 011001.
- [10] Andre K Geim and Konstantin S Novoselov. "The rise of graphene". In: *Nature materials* 6.3 (2007), p. 183.
- [11] Xiaowei Du et al. "Graphene microelectrode arrays for neural activity detection". In: *Journal of biological physics* 41.4 (2015), pp. 339–347.
- [12] Lucas H Hess et al. "Graphene transistor arrays for recording action potentials from electrogenic cells". In: *Advanced Materials* 23.43 (2011), pp. 5045–5049.
- [13] Dong-Wook Park et al. "Graphene-based carbon-layered electrode array technology for neural imaging and optogenetic applications". In: *Nature communications* 5 (2014), ncomms6258.

- [14] Suck Won Hong et al. "Enhanced neural cell adhesion and neurite outgrowth on graphene-based biomimetic substrates". In: *BioMed research international* 2014 (2014).
- [15] Ning Li et al. "Three-dimensional graphene foam as a biocompatible and conductive scaffold for neural stem cells". In: *Scientific reports* 3 (2013), p. 1604.
- [16] Eric R Kandel et al. *Principles of neural science*. Vol. 4. McGraw-hill New York, 2000.
- [17] Steven R Quartz and Terrence J Sejnowski. "The neural basis of cognitive development: A constructivist manifesto". In: *Behavioral and brain sciences* 20.4 (1997), pp. 537–556.
- [18] Larry Squire et al. *Fundamental neuroscience*. Academic Press, 2012.
- [19] OpenStax - Biology. URL: <https://openstax.org/details/books/biology>.
- [20] Eric H Chudler. "Brain facts and figures". In: *Visitada en septiembre de* (2003).
- [21] Charles F Stevens. "The neuron". In: *Scientific American* 241.3 (1979), pp. 54–65.
- [22] B Katz and R Miledi. "A study of synaptic transmission in the absence of nerve impulses". In: *The Journal of physiology* 192.2 (1967), pp. 407–436.
- [23] Danny Banks. "Neurotechnology". In: *Engineering Science and Education Journal* 7.3 (1998), pp. 135–144.
- [24] *MedBullets. Step1 - Neurology*. URL: <http://step1.medbullets.com/>.
- [25] Julius Axelrod. "Neurotransmitters". In: *Scientific American* 230.6 (1974), pp. 58–71.
- [26] Darrell A Henze et al. "Intracellular features predicted by extracellular recordings in the hippocampus in vivo". In: *Journal of neurophysiology* 84.1 (2000), pp. 390–400.
- [27] György Buzsáki et al. "Tools for probing local circuits: high-density silicon probes combined with optogenetics". In: *Neuron* 86.1 (2015), pp. 92–105.
- [28] György Buzsáki. "Large-scale recording of neuronal ensembles". In: *Nature neuroscience* 7.5 (2004), p. 446.
- [29] Bruce L McNaughton, John O'Keefe, and Carol A Barnes. "The stereotrode: a new technique for simultaneous isolation of several single units in the central nervous system from multiple unit records". In: *Journal of neuroscience methods* 8.4 (1983), pp. 391–397.
- [30] John P Donoghue. "Connecting cortex to machines: recent advances in brain interfaces". In: *Nature neuroscience* 5 (2002), p. 1085.
- [31] Francis HC Crick. "Thinking about the brain". In: *Scientific American* 241.3 (1979), pp. 219–233.
- [32] Xu Liu and Susumu Tonegawa. "Optogenetics 3.0". In: *Cell* 141.1 (2010), pp. 22–24.
- [33] Lief Fenno, Ofer Yizhar, and Karl Deisseroth. "The development and application of optogenetics". In: *Annual review of neuroscience* 34 (2011).

- [34] Christina K Kim, Avishek Adhikari, and Karl Deisseroth. "Integration of optogenetics with complementary methodologies in systems neuroscience". In: *Nature Reviews Neuroscience* 18.4 (2017), p. 222.
- [35] Alexander M Aravanis et al. "An optical neural interface: in vivo control of rodent motor cortex with integrated fiberoptic and optogenetic technology". In: *Journal of neural engineering* 4.3 (2007), S143.
- [36] Jing Wang et al. "A neurophotonic device for stimulation and recording of neural microcircuits". In: *Engineering in Medicine and Biology Society (EMBC), 2010 Annual International Conference of the IEEE*. IEEE. 2010, pp. 2935–2938.
- [37] Khalil Najafi. "Solid-state microsensors for cortical nerve recordings". In: *IEEE engineering in medicine and biology magazine* 13.3 (1994), pp. 375–387.
- [38] Josef Skrzypek and Edward Keller. "Manufacture of metal microelectrodes with the scanning electron microscope". In: *IEEE Transactions on Biomedical Engineering* 5 (1975), pp. 435–437.
- [39] Richard A Normann et al. "A neural interface for a cortical vision prosthesis". In: *Vision research* 39.15 (1999), pp. 2577–2587.
- [40] Kensall D Wise et al. "Wireless implantable microsystems: high-density electronic interfaces to the nervous system". In: *Proceedings of the IEEE* 92.1 (2004), pp. 76–97.
- [41] RR Richardson Jr, JA Miller, and William M Reichert. "Polyimides as biomaterials: preliminary biocompatibility testing". In: *Biomaterials* 14.8 (1993), pp. 627–635.
- [42] Shoji Takeuchi et al. "3D flexible multichannel neural probe array". In: *Journal of micromechanics and microengineering* 14.1 (2003), p. 104.
- [43] S Kanno et al. "Multiple optical stimulation to neuron using Si opto-neural probe with multiple optical waveguides and metal-cover for optogenetics". In: *Engineering in Medicine and Biology Society (EMBC), 2013 35th Annual International Conference of the IEEE*. IEEE. 2013, pp. 253–256.
- [44] Anthony N Zorzos, Edward S Boyden, and Clifton G Fonstad. "Multiwaveguide implantable probe for light delivery to sets of distributed brain targets". In: *Optics letters* 35.24 (2010), pp. 4133–4135.
- [45] Eran Segev et al. "Patterned photostimulation via visible-wavelength photonic probes for deep brain optogenetics". In: *Neurophotonics* 4.1 (2016), p. 011002.
- [46] Michael L Roukes, Trevor Fowler, and Jessica L Arlett. *Highly multiplexed optogenetic neural stimulation using integrated optical technologies*. US Patent App. 14/086,790. 2014.
- [47] Matthew J Allen, Vincent C Tung, and Richard B Kaner. "Honeycomb carbon: a review of graphene". In: *Chemical reviews* 110.1 (2009), pp. 132–145.
- [48] CH Chen et al. "A graphene-based microelectrode for recording neural signals". In: *Solid-State Sensors, Actuators and Microsystems Conference (TRANSDUCERS), 2011 16th International*. IEEE. 2011, pp. 1883–1886.

- [49] Brianna C Thompson, Eoin Murray, and Gordon G Wallace. "Graphite oxide to graphene. Biomaterials to bionics". In: *Advanced Materials* 27.46 (2015), pp. 7563–7582.
- [50] Z Fekete et al. "Improved process flow for buried channel fabrication in silicon". In: *Microsystem technologies* 18.3 (2012), pp. 353–358.
- [51] IH Malitson. "Interspecimen comparison of the refractive index of fused silica". In: *Josa* 55.10 (1965), pp. 1205–1209.
- [52] *Lionix International*. URL: <https://www.lionix-international.com/>.
- [53] *Brewer Science*. URL: <https://www.brewerscience.com/products/rotek-psb/>.
- [54] Zuwei Liu et al. "Super-selective cryogenic etching for sub-10 nm features". In: *Nanotechnology* 24.1 (2012), p. 015305.
- [55] Xuesong Li et al. "Evolution of graphene growth on Ni and Cu by carbon isotope labeling". In: *Nano letters* 9.12 (2009), pp. 4268–4272.
- [56] Cecilia Mattevi, Hokwon Kim, and Manish Chhowalla. "A review of chemical vapour deposition of graphene on copper". In: *Journal of Materials Chemistry* 21.10 (2011), pp. 3324–3334.
- [57] Martin Benjamin Barbour Spangat Larsen. "Chemical Vapor Deposition of Large Area Graphene". PhD Thesis. Technical University of Denmark, 2015.
- [58] Soo Min Kim et al. "The effect of copper pre-cleaning on graphene synthesis". In: *Nanotechnology* 24.36 (2013), p. 365602.
- [59] S Chaitoglou and E Bertran. "Effect of pressure and hydrogen flow in nucleation density and morphology of graphene bidimensional crystals". In: *Materials Research Express* 3.7 (2016), p. 075603.
- [60] Stefanos Chaitoglou et al. "Effect of a balanced concentration of hydrogen on graphene CVD growth". In: *Journal of Nanomaterials* 2016 (2016), p. 54.
- [61] Stefanos Chaitoglou and Enric Bertran. "Effect of temperature on graphene grown by chemical vapor deposition". In: *Journal of Materials Science* 52.13 (2017), pp. 8348–8356.
- [62] Neuralynx. *NanoZ User Manual*.
- [63] Carolina Mora Lopez et al. "An implantable 455-active-electrode 52-channel CMOS neural probe". In: *IEEE Journal of Solid-State Circuits* 49.1 (2014), pp. 248–261.
- [64] You-Yin Chen et al. "Design and fabrication of a polyimide-based microelectrode array: application in neural recording and repeatable electrolytic lesion in rat brain". In: *Journal of neuroscience methods* 182.1 (2009), pp. 6–16.
- [65] Micha E Spira and Aviad Hai. "Multi-electrode array technologies for neuroscience and cardiology". In: *Nature nanotechnology* 8.2 (2013), p. 83.
-

## *Acknowledgements*

I would like to thank Stefano Cabrini who gave me the opportunity of working at the Molecular Foundry. He was a stimulating supervisor, always kind and helpful in clarifying my doubts and advising me on how to independently work in a laboratory and efficiently carry on a project.

I thank Vittorino Lanzio who was able to share all his knowledge and make me confident in working in the cleanroom, being always willing to help me with my issues, re-explaining how to carry on the work and working next to me whenever I needed it. He was not only a workmate, but especially a great friend, who helped me to enjoy the life of the laboratory, often waiting with me until late at night, but also the Californian life outside the Foundry.

I thank Gianni Presti and Fabrizio Riminucci to share with me each Californian day, inside and outside the laboratory, encouraging me during the bad ones and joining me in each funny Californian adventure.

I thank Tev K, who helped me for all the graphene part of the project, always making the laboratory days funny but at the same time brain stimulating.

I thank Scott Dhuey who runs the electron beam lithography exposures, always giving me great advice for the implementation of my project.

I thank Michael Elowson for the tool trainings and for listening to my requests and trying to satisfy them even during the busiest days.

Finally I want to really thank Andrea Lamberti for being my thesis supervisor, following me from Italy during all my stay, answering all my questions and teaching me to never lose the enthusiasm in the work that I was developing.